RESEARCH ARTICLE

AMERICAN JOURNAL OF
BIOLOGICAL ANTHROPOLOGY
The Official Journal of the American Association of Biological Anthropologists

WILEY

Sagittal suture strain in capuchin monkeys (*Sapajus* and *Cebus*) during feeding

Craig Byron[1] | David Reed[2] | Jose Iriarte-Diaz[3] | Qian Wang[4] |
David Strait[5,6] | Myra F. Laird[7] | Callum F. Ross[8]

[1]Department of Biology, Mercer University, Macon, Georgia, USA

[2]Department of Oral Biology, University of Illinois, Chicago, Illinois, USA

[3]Department of Biology, University of the South, Sewanee, Tennessee, USA

[4]Department of Biomedical Sciences, Texas A&M University College of Dentistry, Dallas, Texas, USA

[5]Department of Anthropology, Washington University in St. Louis, St. Louis, Missouri, USA

[6]Palaeo-Research Institute, University of Johannesburg, Johannesburg, South Africa

[7]Department of Basic and Translational Sciences, School of Dental Medicine, University of Pennsylvania, Philadelphia, Pennsylvania, USA

[8]Department of Organismal Biology and Anatomy, University of Chicago, Chicago, Illinois, USA

Correspondence
Craig Byron, Department of Biology, Mercer University, 1501 Mercer University Drive, Macon, GA 31207, USA.
Email: byron_cd@mercer.edu

Abstract

Objectives: Morphological variation in cranial sutures is used to infer aspects of primate feeding behavior, including diet, but strain regimes across sutures are not well documented. Our aim is to test hypotheses about sagittal suture morphology, strain regime, feeding behavior, and muscle activity relationships in robust *Sapajus* and gracile *Cebus* capuchin primates.

Materials and Methods: Morphometrics of sinuosity in three regions of the sagittal suture were compared among museum specimens of *Sapajus* and *Cebus*, as well as in robust and gracile lab specimens. In vivo strains and bilateral electromyographic (EMG) activity were recorded from these regions in the temporalis muscles of capuchin primates while they fed on mechanically-varying foods.

Results: *Sapajus* and the anterior suture region exhibited greater sinuosity than *Cebus* and posterior regions. In vivo data reveal minor differences in strain regime between robust and gracile phenotypes but show higher strain magnitudes in the middle suture region and higher tensile strains anteriorly. After gage location, feeding behavior has the most consistent and strongest impact on strain regime in the sagittal suture. Strain in the anterior suture has a high tension to compression ratio compared to the posterior region, especially during forceful biting in the robust *Sapajus*-like individual.

Discussion: Sagittal suture complexity in robust capuchins likely reflects feeding behaviors associated with mechanically challenging foods. Sutural strain regimes in other anthropoid primates may also be affected by activity in feeding muscles.

KEYWORDS
Cebus, cranial sutures, *Sapajus*, strain gage, temporalis

1 | INTRODUCTION

Cranial sutures are connective tissue articulations between the dermal bones of the vertebrate skull comprised of a dense regular extracellular matrix with collagen bundles and fibroblasts. Several different suture morphologies are observed, including straight (or butt-ended), beveled, and waveform. The ectocranial surfaces of waveform sutures are made up of interdigitating convex and concave bony lingulae. The sinuous morphology that results from alternating bone deposition and

2 | WILEY AMERICAN JOURNAL OF BIOLOGICAL ANTHROPOLOGY
The Official Journal of the American Association of Biological Anthropologists

BYRON ET AL.

resorption along convex and concave surfaces suggests morphogenetic coordination across the suture during growth (Byron, 2006; Byron et al., 2004; Khonsari et al., 2013; Zollikofer & Weissmann, 2011). This growth is putatively influenced by strain and deformation regimes in the suture (Moss, 1997a, 1997b, 1997c, 1997d) and suggests that relationships between suture morphology, strain regime and behavior may inform functional interpretation of cranial morphology in extant and fossil vertebrates (Markey et al., 2006; Markey & Marshall, 2007a, 2007b; Rak, 1978; Rak & Kimbel, 1991).

Ectocranial suture sinuosity has been related to the absorption of impact loads during head-butting behaviors, for example in goats (*Capra hircus*; Farke, 2008, Jaslow, 1990, Jaslow & Biewener, 1995), but in most vertebrates, the repeated loading and strain regimes associated with normal feeding are thought to be stronger influences on sutural morphology. Among caiman alligatorids, *Caiman latirostris* eats harder foods than *Caiman sclerops* and has more sinuous facial sutures along its snout (Monteiro & Lessa, 2000). Myostatin deficient, hypermuscular mice have increased sinuosity of the sagittal suture compared with controls (Byron et al., 2004) and mice with masticatory overuse show increased sinuosity posteriorly (Byron et al., 2018). In human archeological populations, relationships between sagittal suture morphology and the increase in extra-oral food processing techniques following the Mesolithic period are weak at best (Cheronet et al., 2021). In nonhuman primates, *Sapajus apella* consumes mechanically resistant foods (i.e., foods that are very stiff and/or crack resistant) and has more sinuous sagittal sutures than those of capuchins that avoid the most mechanically resistant plant tissues, such as *Cebus albifrons* (Byron, 2009).

In vitro and finite element modeling studies provide valuable insights into the impact of sutures on cranial mechanics (Jaslow & Biewener, 1995; Markey et al., 2006; Markey & Marshall, 2007a, 2007b; Moazen et al., 2009; Smith & Hylander, 1985; Wang et al., 2010, 2012), but in vivo data are crucial for understanding the relationships between sagittal sutural morphology and strain regime. Behrents et al. (1978) used single element gages to record laterally directed tensile strains across the anterior third of the sagittal suture of macaques during temporalis muscle stimulation. Behrents et al. data were collected during muscle stimulation, not during natural feeding, making their results minimally relevant to questions about sutural morphology, sutural strain, and feeding behavior. Single element gages are also of limited value for detailed quantification of sutural strain regime because they only record strain magnitudes along the long axes of the gages: they do not provide information on principal strain orientations and magnitudes. Rosette strain gages have been used to record the planar strain state—principal and shear strains—across the external surface of cranial sutures during muscle stimulation and chewing in macaques (Bourbon, 1982), minipigs (Herring & Mucci, 1991; Herring & Teng, 2000; Rafferty & Herring, 1999) and hyraxes (Lieberman et al., 2004). During chewing by macaques maximum principal (tensile) strain orientations were oblique to the long axis of the sagittal suture, suggestive of shear or

twisting of the suture, and compressive strains were orthogonal to the squamous suture, indicating superoinferior compression (Bourbon, 1982). Activation of temporalis during feeding or muscle stimulation in miniature swine pulled the posterior ends of the parietal bones apart and pushed their rostral ends together, and strain regimes along the sagittal suture indicated twisting of the frontal and parietal bones (Herring, 1972, Herring & Mucci, 1991, Rafferty & Herring, 1999, Sun et al., 2004). Clearly in vivo strain data across the sagittal suture during natural feeding are needed to evaluate links between sutural morphology and feeding behavior.

In this study, we characterized the strain regimes during feeding at three locations along the sagittal sutures of two robust, tufted capuchins and two gracile, un-tufted capuchins. Although the individuals could not be definitively assigned to species, the cranial phenotypes suggest the tufted forms are *Sapajus* sp. and the untufted forms represent *Cebus* sp. The more robust morphology of *Sapajus* relative to *Cebus* is characterized by larger teeth, thicker mandibular corpora and symphyses, prominent and anteriorly positioned feeding muscles, greater temporalis physiological cross-sectional area, and more sinuous sagittal sutures (Figure 1; Anapol & Lee, 1994; Byron, 2009; Chai, 2020; Daegling, 1992; Kinzey, 1974; Masterson, 1997; Hogg and Elokda, 2021; Silva Jr., 2001, 2002; Spencer, 2003; Taylor & Vinyard, 2009; Teaford et al., 2020; Wright, 2005). These features are probable adaptations for consumption of tougher foods in *Sapajus* relative to *Cebus*, and a seed predation strategy including obdurate foods, such as palm nuts (Cole, 1992; Defler, 1979a; Defler, 1979b; Freese et al., 1981; Izawa, 1979; Kinzey, 1974; Teaford, 1985; Teaford et al., 2020; Wright, 2005).

The general exploitation of tough foods by *S. apella* is associated with increased sutural sinuosity (Byron, 2009). This assumes that, as in the mandible (Ross et al., 2016), variation in food materials properties is associated with variation in some aspect of feeding behavior, such as bite and muscle force magnitudes, bite point, biting side, biting versus chewing cycles, and/or use of the hands during ingestive behaviors (Laird, Wright, et al., 2020; Ross et al., 2016). These behaviors are expected to vary sagittal suture strain magnitudes and orientations, as well as temporalis muscle activation patterns, which elicit a growth response that alters the adult sutural phenotype.

> **Hypothesis 1.** Suture structure and function vary with location, food materials properties, and feeding behavior.

Sutural and strain variability are addressed through two specific predictions. The null hypothesis is that sagittal suture sinuosity is homogenous among locations, and that strains are purely laterally directed, homogeneous along the suture, and homogeneous across food materials properties, feeding behaviors, and cranial phenotypes. We were agnostic about the orientation (other than a lateral direction) of sutural strains along the sagittal suture.
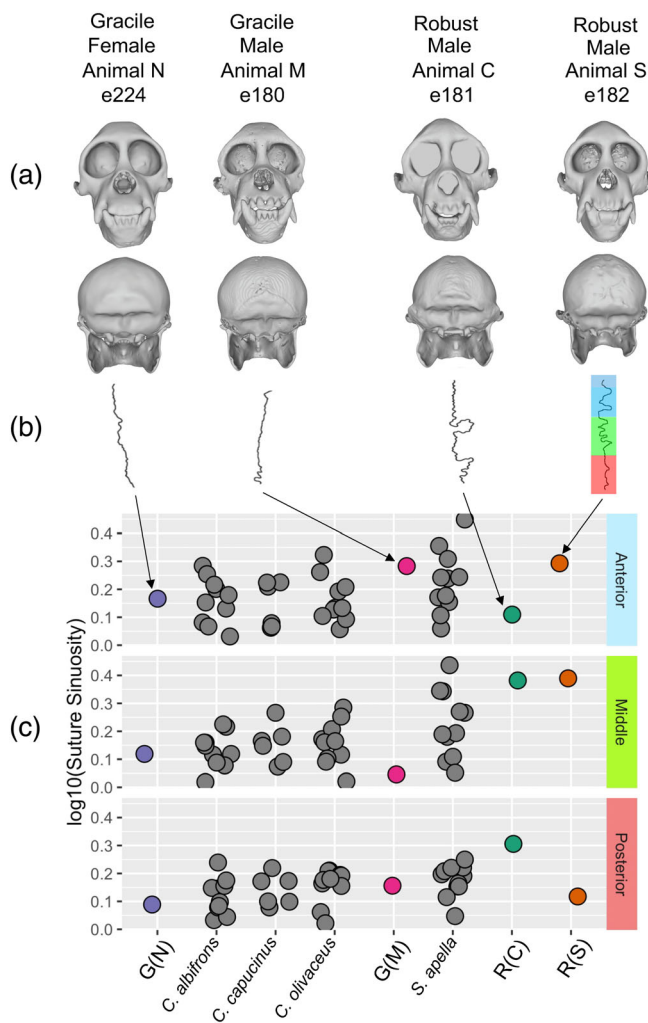
BYRON ET AL.

AMERICAN JOURNAL OF **BIOLOGICAL ANTHROPOLOGY** The Official Journal of the American Association of Biological Anthropologists —WILEY— 3

FIGURE 1 Experimental sample. (a) Rostral and caudal views from 3D renders of CT scans representing experimental animals-Prediction 1.1. (b) Tracings from the ectocranial appearance of sagittal sutures in experimental animals. (c) Log₁₀ suture sinuosity measurement in the museum sample and experimental animals.

Prediction 1.1: Suture morphology (sinuosity, amplitude, and spacing-i.e., complexity) differs between the anterior, middle, and posterior regions of sagittal suture.

Prediction 1.2: In robust and gracile capuchins strain regime varies with gage location and in relation to food materials properties and feeding behavior.

Hypothesis 2. Temporalis regions differentially contribute to sutural strain.

The second goal of this paper is to compare the contributions of temporalis activation to strain regimes at the sagittal suture (Dzialo et al., 2014; Herring & Teng, 2000; Rak, 1978; Rak & Kimbel, 1991). Temporalis activation varies between the muscle's anterior and posterior regions and between the working (loading) and balancing (non-loading) sides (Hylander et al., 2005; Ram &

Ross, 2018; Vinyard, 2007; Vinyard, 2008; Vinyard et al., 2008; Wall et al., 2008). In primates studied to date, activity in the working side posterior temporalis (WPT) peaks before that in the balancing side posterior temporalis (BPT) but after the balancing side anterior temporalis (BAT) (Hylander et al., 2005; Ram & Ross, 2018; Vinyard, 2007; Vinyard, 2008; Vinyard et al., 2008; Wall et al., 2008). These timing differences make it possible to evaluate contributions of different parts of temporalis to strain regime in the sagittal suture. In capuchins, the frontal bone extends so far posteriorly that the sagittal suture is adjacent to only the posterior temporalis. The null hypothesis is that temporalis activation is not associated with strain regime locations along the sagittal suture or with side-related changes in strain regimes.

Prediction 2.1: Posterior temporalis activity better explains the variance in sagittal suture strain regime during feeding than the anterior temporalis.

Prediction 2.2: Chewing side-related variation in relative timing of working and balancing posterior temporalis activity is associated with side-related variation in strain regime.

2 | MATERIALS AND METHODS

2.1 | Suture morphology measures (Prediction 1.1)

Three suture metrics were quantified in the four in vivo subject animals, as well as in a sample of 32 adult male capuchin specimens accessioned in the Field Museum of Natural History, Chicago, IL as one of four species: *Sapajus apella*, *Cebus albifrons*, *Cebus capucinus*, and *Cebus olivaceus*. Only males were selected for the museum sample because they generally show a more robust cranial phenotype than females in each taxon (Masterson, 1997). Sinuosity was quantified from digital image tracings of the sagittal sutures using a modified measure of relative suture length (Byron, 2009; Byron et al., 2004; Jaslow, 1990). Using ImageJ (version 2.1.0) a chord (i.e., straight line between two points) was drawn from the front (bregma) to the back (lambda) of each sagittal suture (herein, "Chord length"). Anterior, middle, and posterior thirds of the suture were distinguished in ImageJ using a custom script that creates three even line segments from any chord. Then, freehand lines ("Suture path length") were traced for each suture third. These regions of interest were measured and results saved for chord length and path length so that a relative length measure could be compared between each of the three sagittal suture regions

$$\text{Sinuosity} - \text{Relative Length}\,(\%) = \text{Suture Path Length}/\text{Chord Length}$$

Sutures from experimental subjects were traced from micro-CT (micro-computed tomography) images or photos taken during surgery (Figure 1). The authors have no data to suggest there are differences in suture tracings between micro-CT and digital photo derived sources. There are data however, that tracings made from a two-dimensional surface (i.e., photo) yield slightly larger values of suture sinuosity than tracings made with adhesive tape on the surface of the

4 | WILEY–**AMERICAN JOURNAL OF BIOLOGICAL ANTHROPOLOGY** The Official Journal of the American Association of Biological Anthropologists

BYRON ET AL.

cranium (Byron, 2009). In order to measure the amplitude and spacing of each suture region the .roi files from ImageJ were read into R using the package RImageJROI (Sterratt & Vihtakari, 2021) and the suture region XY coordinates were aligned to the mean. Peaks/valleys were defined as up or down changes greater than 3, and spacing greater than 3 along the suture path. Changes in spacing between peaks/valleys and amplitude relative to chord length were compared across genus/phenotype, sex, and sagittal suture region.

2.2 | In vivo data collection (Predictions 1.2, 2.1, and 2.2)

Data were collected from four individual capuchins (C, M, N, and S) during four recording sessions (experiments e224 [animal C], e180 [M], e181 [N], e182 [S]; Figure 1). Individual N was female, the others were males. All animals were mature adults with the third molar in occlusion. N and M were gracile and C and S were robust with more prominent supraorbital tori, laterally flaring mandibular rami, more acute mandibular angles, wider zygomas, more distinct lines of temporalis origin, and greater postorbital constriction of the calvaria. None of the animals displayed sagittal cresting so a patent and accessible suture was available in each without a need to reflect the temporalis muscle away from the temporal lines on the parietal bones. In this paper, each animal will be given a specimen designation that also denotes gracile vs. robust cranial phenotype: G(M), G(N), R(C), and R(S). The animals had previously been trained with operant conditioning to feed while seated in a primate chair (Laird et al., in prep; Laird, Granatosky, et al., 2020; Ross et al., 2016). This experimental protocol and procedure was ethically reviewed and approved by UChicago IACUC (Institutional Care and Use Committee) ACUP (Animal Care and Use Protocol) #72382. Results were obtained in accordance with relevant institutional and national guidelines for the care and use of laboratory animals.

Delta rosette strain gages (SA-06-030WY-120, Micromeasurements, Raleigh, NC) wired in a three-wire quarter-bridge circuit were used to record strains across the sagittal suture in anterior (adjacent to bregma), middle (the visually inspected midpoint between the terminal locations), and posterior (adjacent to lambda) locations (Figure 2). The animals were food-deprived for 24 h before each experiment, sedated using an intramuscular injection of ketamine and medetomidine then anesthetized using inhalant isoflurane (Theriault et al., 2008). Medetomidine was reversed with atipamezole soon after induction of anesthesia; at least 3 h elapsed after ketamine administration before data were recorded. Under isofluorane anesthesia a single incision was made in the skin overlying the sagittal suture, the periosteum elevated to expose the bone, a small area of cortical bone and suture degreased with clinical grade chloroform, then the rosettes bonded across the sagittal suture with a cyanoacrylate adhesive. The gages were separated from the underlying sutural tissue by a thin strip of Teflon tape to keep sutures free of adhesive (Herring & Mucci, 1991) and the lead wires were bonded to the bone for 3–4 mm (millimeters) for strain relief. These steps underscore another notable reality to sutural strain gage experiments in the literature, that the quality of gage installations may vary across studies and disagreement in sutural strain estimates could be methodological rather than an effect of sampled species, locations, or ages. The incision was sutured closed around the lead wires and radiographs taken to document strain gage position and orientation.

The monkeys were seated in a commercially available chair (XPL-517-CM, Plas Labs, Lansing, MI) modified to allow the head and neck to move freely and to allow the animals to use their arms and hands to feed themselves during data recording (Reed & Ross, 2010; Ross et al., 2016). Each of the three elements of the rosette gages was connected to form one arm of a Wheatstone Bridge, with bridge excitation at two volts. Voltage changes were conditioned and amplified on a Vishay 2120 system, and then recorded at 2 kHz (kilohertz) and synchronized with digital video records using MiDAS 2.0 (Xcitex, Cambridge, MA). Videos of animal behavior and jaw kinematics were recorded using a Vicon 10-camera MX T40 system (Culver City, CA).

Strains were recorded while the animals ingested and masticated stress-limited foods (foods of high toughness and high stiffness, i.e., Brazil nuts, walnuts, and almonds) and displacement-limited foods (foods of high toughness and low stiffness, apricots and grapes), foods shown previously to alter capuchin chewing behavior (Reed & Ross, 2010). Masticatory cycle types designated "nut shell" correspond to sequences in which the animals fractured the outer seed coating. Cycle types designated as "nut" are sequences in which the animals ate the nut kernel. Cycle types designated as "fruit" correspond to sequences in which the animals ate displacement-limited food items such as apricots and grapes. For this analysis, Brazil nuts and walnuts included the shell, which elicited forceful cracking of the outer seed coat prior to mastication of the softer kernel. The nuts were relatively large, with diameters of 15–25 mm, resulting in large gape behaviors during ingestive biting. After the recording sessions each animal was anesthetized, the gages were removed, the site cleaned and sutured closed, analgesics and antibiotics administered, and the animal returned to its cage. All animals recovered without complications.
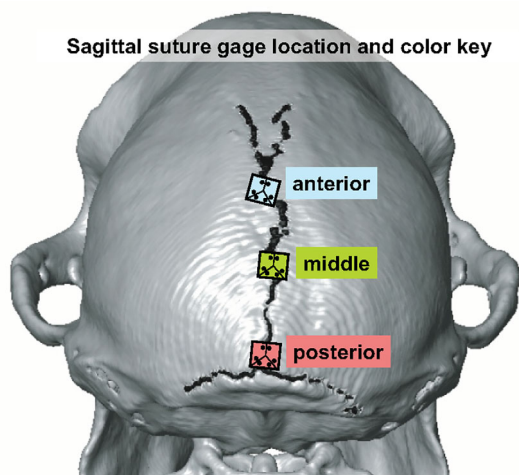

FIGURE 2 Location of strain gages on sagittal suture of Animal S and color key for following figures.

AMERICAN JOURNAL OF BIOLOGICAL ANTHROPOLOGY
The Official Journal of the American Association of Biological Anthropologists

WILEY 5

The strain data and videos were examined to identify movement artifacts, feeding behaviors—incisor, canine, premolar, molar ingestion bites, and mastication cycles—and chewing side following Ross et al. (2016). Sequences were selected for analysis on the basis of clarity of food processing behaviors. Gape cycles were excluded if the magnitudes of the strains decreased so as to be unreliably distinguishable from noise (5–10 mV, millivolts, in each channel). To sample the diversity of feeding behaviors, all gape cycles for which cycle type could be identified were analyzed. The complexity of the experimental design, and the naturalistic feeding data that we sought, resulted in unevenness in data collection. For example, we have a greater amount of data from robust individuals than from gracile ones. There were fewer useful gape cycles processing nutshells, or for specimen G(M) cycle types other than chewing. For the lone female specimen G(N) data were not successfully recorded from the anterior gage. The statistical methods selected help offset these challenges, but it remains a possibility that some aspects of our results are related to these unequal samples.

2.3 | Strain data analysis (Predictions 1.2, 2.1, and 2.2)

Strain data were processed in IGOR Pro 4.0 (WaveMetrics, Inc., Lake Oswego, OR) using custom written software. The strain data were resampled at a rate of 1 kHz then converted to microstrain (με) using calibration files made during the recording sessions. Strain (ε), a dimensionless variable equaling the change in length of an object divided by its original length, is measured in microstrain (με). Tensile strain is registered as a positive value and compressive strain as a negative value. The maximum principal strains are the largest tensile strain values (ε_1). The minimum principal strains are the largest compressive strain values (ε_2). Strain mode ($\varepsilon_1/\varepsilon_2$) was used as an estimate of strain regime with high tensile strain modes as $\varepsilon_1 \geq 200\%$ of ε_2, high compressive strain modes as $\varepsilon_1 \leq 50\%$ of ε_2, and shear when the ε_1 and ε_2 magnitudes are within 50% of each other. Following Smith et al. (2015), we used the $\log_{10}$ transformation of this ratio so that values $\geq +0.301$ represent high tension, values ≤ -0.301 represent high compression, and values between $+0.176$ and -0.176 represent shear. The orientation of the maximum principal strain was calculated relative to the mid-sagittal plane, with 0 degrees being perpendicular to the sagittal plane and to the right. Strain orientations were transformed to plot on a coordinate space that is 90–270° (i.e., to the left side of the sagittal suture if viewed from the posterior aspect). Raw angular data from the 90–270° coordinate space were then radian-transformed for their summary and inferential statistics (see below).

2.4 | EMG data analysis (Predictions 2.1 and 2.2)

Indwelling fine-wire electrodes were placed bilaterally in the superficial masseter (10 mm from the inferior border of the mandible), and at three locations along the temporalis muscle: anterior, middle, and posterior. Electrodes in the temporalis were placed 10 mm inferior to the temporal line by inserting the needle in a coronal plane at an angle of approximately 45° to the sagittal plane until it contacted bone. Raw EMG (electromyography) signals were sampled at a rate of 2 kHz and band-pass filtered (100–2000 Hz, Hertz), then converted to smoothed, rectified waves using a root mean square algorithm with a 42 ms time constant in 2 ms increments (Hylander & Johnson, 1985). For each chewing cycle, the relative timing and amplitude of peak EMG in each muscle was calculated, and the relative timing of 75%, 50%, and 25% of peak prior to and following peak were extracted and plotted. In this type of plot, muscle timing data were standardized relative to the firing of the working side superficial masseter. It is worth noting that muscle activity as recorded with EMG is not the same as muscular force. Thus, to relate muscle output to maximum principal strain, EMG amplitude data were normalized through dividing them by the largest EMG amplitude recorded from each electrode during the entire day's experiment.

2.5 | Statistical methods

Data were analyzed in R 3.6.2, RStudio 1.1.456 using the tidyverse, circular, CircStats, lme4, multcomp, relaimpo, lmerTest, and bpnreg packages (Agostinelli & Lund, 2017; Bates et al., 2015; Cremers, 2018; Grömping, 2006; Hothorn et al., 2008; Kuznetsova et al., 2017; R Core Team, 2020; Wickham et al., 2019). With all inferential statistics, p-values that reject the null hypothesis beyond the 0.05 level are reported as significant. Anything lower than 0.01 (i.e., 0.001 and 0.0001) is considered to be highly significant.

Prediction 1.1: Sagittal suture complexity (sinuosity, relative amplitude, and relative spacing) was compared using a two-way ANOVA (analysis of variance) with suture metric as the dependent variable and genus identity (*Sapajus* vs. *Cebus*) and suture region (anterior vs. middle vs. posterior) as independent variables. Post-hoc Tukey tests were conducted to determine how all combinations of genus and suture region compared to one another.

Prediction 1.2: A mixed effects ANOVA model was used to analyze the variance in three dependent strain variables quantifying strain regime: ε_1 and ε_2 magnitudes, and strain mode. Variation in each variable was examined using an increasing series of more complicated linear models that included both fixed and random effects (i.e., independent variables). Model construction began by adding the two random effects (individual and food item type) followed by each of the five fixed effects (gage site, cycle type, chew side, cranial phenotype, and sex). Proceeding in a stepwise manner, AIC (Akaike's "An Information Criterion") was reported as lower values incrementally indicating that as random and fixed effects were introduced the model explained more of the variance in the dependent strain variable. All models were significantly improved by including all these effects.

6 | WILEY AMERICAN JOURNAL OF BIOLOGICAL ANTHROPOLOGY
The Official Journal of the American Association of Biological Anthropologists

BYRON ET AL.

Generalized linear mixed model

$$\leftarrow \text{lmer(Strain Regime Variable} \sim (1|\text{individual})$$
$$+ (1|\text{food item type}) + \text{gage site} + \text{cycle type}$$
$$+ \text{chew side} + \text{cranial phenotype} + \text{sex, data} = .)$$

Each effect had multiple levels, as follows: individual (four experimental subjects, G(M), G(N), R(C), and R(S)); sex (male or female), cranial phenotype (gracile or robust), food type (fruit, nut, or nutshell); chew side (left or right); cycle type (incisor bite, canine bite, premolar bite, molar bite, and chew); and gage site, or location along the sagittal suture (anterior, adjacent to bregma; middle, midway between bregma and lambda; posterior, adjacent to lambda). The lmer() and associated ANOVA and ANOVA-like functions return a likelihood ratio test statistic (LRT) for each random effect and an F-statistic for each fixed effect. Relative magnitudes of these statistics and p-values were used to assess significance of effects on strain regime. Estimates of fixed effect levels relative to other levels from that effect included a measure of statistical significance.

The strain orientation data of ε_1 were analyzed with a mixed effects model designed for circular data following Cremers and Klugkist (2018). The model was constructed by serially adding fixed effects (chew side, gage site, cycle type, cranial phenotype, and sex) to a model initialized with the individual level specified as a random effect. Model building proceeds step-wise with each new effect added and its DIC (Deviance Information Criterion) statistic. This information criterion statistic decreased after adding all effects except for sex. Adding sex as a fixed effect did not increase the DIC value eliminating it as the best model for the orientation data. Thus, the model that accounts for most variation, and also lends itself to more straightforward interpretation, includes all combinations of these fixed effects except sex (30 combinations of effect levels).

Circular mixed effects model $\leftarrow$ bpnme(pred.I
$$= \text{radian\_degree} \sim (1|\text{individual}) + \text{side} + \text{location} + \text{cycle type}$$
$$+ \text{cranial phenotype, data} = ., \text{its} = 10000, \text{burn} = 1000, \text{n.lag} = 3,$$
$$\text{seed} = 101)$$

TABLE 1 Results of tests for heterogeneity in suture sinuosity-Prediction 1.1.

	Degrees of freedom	Sum Sq	Mean Sq	F-value	p-value
Genus	1	0.087	0.087	13.6	**<0.001**
Suture region	2	0.017	0.008	1.3	NS
Genus:Suture region	2	0.008	0.004	0.602	NS
Residuals	105	0.673	0.006		
Tukey-tests					

	Estimated difference	p-value
Sapajus-Cebus	0.061	**<0.001**
Middle – Anterior	−0.008	NS
Posterior – Anterior	−0.029	NS
Posterior – Middle	−0.021	NS
Sapajus:Anterior – *Cebus*:Anterior	0.07	NS
Cebus:Middle – *Cebus*:Anterior	−0.01	NS
Sapajus:Middle – *Cebus*:Anterior	0.067	NS
Cebus:Posterior – *Cebus*:Anterior	−0.019	NS
Sapajus:Posterior – *Cebus*:Anterior	0.017	NS
Cebus:Middle – *Sapajus*:Anterior	−0.081	NS
Sapajus:Middle – *Sapajus*:Anterior	−0.003	NS
Cebus:Posterior – *Sapajus*:Anterior	−0.089	**<0.05**
Sapajus:Posterior – *Sapajus*:Anterior	−0.053	NS
Sapajus:Middle – *Cebus*:Middle	0.078	NS
Cebus:Posterior – *Cebus*:Middle	−0.008	NS
Sapajus:Posterior – *Cebus*:Middle	0.027	NS
Cebus:Posterior – *Sapajus*:Middle	−0.086	**<0.05**
Sapajus:Posterior – *Sapajus*:Middle	−0.05	NS
Sapajus:Posterior – *Cebus*:Posterior	0.036	NS

Note: All bold values represent statistical significance at the correspondingly listed p-value that is 0.05 or lower.

TABLE 2 Results of tests for heterogeneity in suture amplitude to chord length-Prediction 1.1.

	Degrees of freedom	Sum Sq	Mean Sq	F-value	*p*-value
Genus	1	0.396	0.396	74.9	**<0.0001**
Suture Region	2	0.036	0.018	3.44	**<0.05**
Genus:Suture region	2	0.108	0.054	10.3	**<0.001**
Residuals	1667	8.806	0.005		
Tukey-tests					

	Estimated difference	*p*-value
Sapajus-Cebus	0.036	**<0.0001**
Middle – Anterior	−0.001	NS
Posterior – Anterior	−0.01	**<0.05**
Posterior – Middle	−0.009	NS
Sapajus:Anterior – *Cebus*:Anterior	0.028	**<0.01**
Cebus:Middle – *Cebus*:Anterior	−0.009	NS
Sapajus:Middle – *Cebus*:Anterior	0.056	**<0.0001**
Cebus:Posterior – *Cebus*:Anterior	−0.008	NS
Sapajus:Posterior – *Cebus*:Anterior	0.014	NS
Cebus:Middle – *Sapajus*:Anterior	−0.037	**<0.0001**
Sapajus:Middle – *Sapajus*:Anterior	0.029	**<0.05**
Cebus:Posterior – *Sapajus*:Anterior	−0.036	**<0.0001**
Sapajus:Posterior – *Sapajus*:Anterior	−0.014	NS
Sapajus:Middle – *Cebus*:Middle	0.066	**<0.0001**
Cebus:Posterior – *Cebus*:Middle	0.001	NS
Sapajus:Posterior – *Cebus*:Middle	0.023	**<0.01**
Cebus:Posterior – *Sapajus*:Middle	−0.065	**<0.0001**
Sapajus:Posterior – *Sapajus*:Middle	−0.042	**<0.0001**
Sapajus:Posterior – *Cebus*:Posterior	0.022	**<0.05**

To test Prediction 1.2—that strain regime varies with location in the sagittal suture, with chewing side, with feeding behavior, and with food material properties—we tested for significant effects of these variables in our ANOVA.

Prediction 2.1 and 2.2: Peak EMG activity was first ordered in the working and balancing temporalis, and chew side was categorized as working- and balancing-side by comparing the left and right EMG activity. Differences in the timing of working- and balancing-side anterior temporalis and posterior temporalis peak amplitude were tested using ANOVA and pairwise Tukey comparisons. We then used a multiple regression analysis to evaluate how each peak amplitude from the left and right temporalis predicts maximum principal strain magnitude at the anterior, middle, and posterior gage locations.

$$\text{Multiple regression model} \leftarrow \text{lm}(\text{maximum principal strain} \sim \text{RATP} + \text{LATP} + \text{RMTP} + \text{LMTP} + \text{RPTP} + \text{LPTP}, \text{data} = .)$$

The resulting model coefficients were compared using the calc. relimp() function to determine the relative importance of each independent variable (EMG) in the model. The two metrics used here were the Beta Squared method which is the squared standardized coefficient and the Genizi method which is the R^2 decomposition (Genizi, 1993).

3 | RESULTS

3.1 | Prediction 1.1: Suture morphology (sinuosity, amplitude, and spacing-i.e., complexity) differs between the anterior, middle, and posterior regions of sagittal suture

Genus identity (*Sapajus* and *Cebus*) has a significant effect on suture sinuosity (F-ratio = 13.6, $P < 0.001$; Table 1; Figure 1b,c). Post-hoc Tukey tests reveal that *Sapajus* sutures have greater sinuosity ($P < 0.001$), and the posterior sagittal suture of *Cebus* is less sinuous than both the anterior and middle regions in *Sapajus* ($P < 0.05$; $P < 0.05$). The most robust individual in our in vivo study, S, had a suture that was very complex overall (Figure 1b) and also more sinuous in its anterior and middle third compared to nearly all other museum and experimental specimens (Figure 1c). Suture region amplitude and spacing are consistent with these results (Tables 2 and 3). *Sapajus* has significantly greater spacing and higher amplitudes than *Cebus* ($P < 0.0001$), and the anterior region has significantly greater spacing and higher amplitudes than the posterior region in both *Sapajus* and *Cebus* ($P < 0.05$). Broadly across factor level contrasts, significant differences are observed between anterior and posterior as well as *Sapajus* and *Cebus* groupings. The other

8 | WILEY_AMERICAN JOURNAL OF BIOLOGICAL ANTHROPOLOGY
The Official Journal of the American Association of Biological Anthropologists

BYRON ET AL.

experimental subjects also exhibited regional sinuosity measures (Figure 1c) consistent with their gracile (G(N) and G(M)) and robust (R(C) and R(S)) cranial phenotypes with posterior regions of the sagittal suture showing the least sinuosity. Summary statistics for suture sinuosity, spacing, and amplitude are provided in Supplementary Data Tables 1–3 respectively. The underlying assumptions of this work—that robust and gracile capuchins differ in sagittal suture sinuosity—is supported and our experimental animals do seem to be representative of the range of morphologies seen in wild capuchins.

3.2 | Prediction 1.2: Strain regimes vary in relation to gage location, food material properties, and feeding behavior in robust and gracile capuchins

The morphological data suggest sinuosity, amplitude, and spacing are not homogenous along the sagittal suture, that is, *Sapajus* middle and anterior suture regions are more sinuous, with higher amplitudes, and greater spacing than in *Cebus* posterior regions. Maximum principal strain (ε_1) magnitude data are presented in Figure 3 (summary statistics are in Supplementary Data Table 4). Minimum principal strain (ε_2)

data are shown in Supplementary Figure 1 (summary statistics are in Supplementary Data Table 5). Principal strain (ε_1 and ε_2) magnitudes were most strongly affected by gage site along the suture (Table 4). The highest principal strain magnitudes were recorded at the middle location ($P < 0.0001$); and anterior and middle locations experienced higher ε_1 (not ε_2) magnitudes than the posterior location (Figure 3; Table 5, $P < 0.001$). Principal strain magnitudes were also significantly affected by cycle type (Table 6; $P < 0.0001$), being highest during premolar biting ($P < 0.001$), then canine biting ($P < 0.001$) and chewing ($P < 0.001$), then incisor biting ($P < 0.001$, Table 5). Cranial phenotype, and sex also affected maximum principal strains but to a lesser degree ($P < 0.05$ and $P < 0.01$ respectively). Bite side did not have a significant effect on ε_1 magnitudes when these other effects were controlled (NS), but it did impact ε_2 magnitudes (Table 6, $P < 0.0001$). Principal strain magnitudes were also significantly affected by food type and "individual", with the food type effects being stronger than individual effects (LRT = 996 vs. 558; $P < 0.0001$; Table 6). Feeding on nuts and nutshells was associated with higher ε_1 and ε_2 magnitudes than fruit feeding, and the two robust individuals (R(C) and R(S)) exhibited higher principal strain magnitudes than the two gracile individuals (G(N) and G(M)) and this was significant in our models (Figure 3; Table 5; estimate = 0.3, $P < 0.001$). Also in our model,

TABLE 3 Results of tests for heterogeneity in suture spacing to chord length-Prediction 1.1.

	Degrees of freedom	Sum Sq	Mean Sq	F-value	p-value
Genus	1	0.256	0.256	19.6	**<0.0001**
Suture region	2	0.099	0.050	3.79	**<0.05**
Genus:Suture region	2	0.187	0.093	7.14	**<0.001**
Residuals	1667	21.8	0.013		
Tukey-tests					

	Estimated difference	p-value
Sapajus-Cebus	0.029	**<0.0001**
Middle – Anterior	−0.005	NS
Posterior – Anterior	−0.018	**<0.05**
Posterior – Middle	−0.013	NS
Sapajus:Anterior – *Cebus*:Anterior	0.055	**<0.001**
Cebus:Middle – *Cebus*:Anterior	−0.003	NS
Sapajus:Middle – *Cebus*:Anterior	0.044	**<0.01**
Cebus:Posterior – *Cebus*:Anterior	−0.005	NS
Sapajus:Posterior – *Cebus*:Anterior	−0.004	NS
Cebus:Middle – *Sapajus*:Anterior	−0.058	**<0.0001**
Sapajus:Middle – *Sapajus*:Anterior	−0.011	NS
Cebus:Posterior – *Sapajus*:Anterior	−0.059	**<0.0001**
Sapajus:Posterior – *Sapajus*:Anterior	−0.059	**<0.001**
Sapajus:Middle – *Cebus*:Middle	0.048	**<0.01**
Cebus:Posterior – *Cebus*:Middle	−0.001	NS
Sapajus:Posterior – *Cebus*:Middle	−0.001	NS
Cebus:Posterior – *Sapajus*:Middle	−0.049	**<0.001**
Sapajus:Posterior – *Sapajus*:Middle	−0.049	**<0.01**
Sapajus:Posterior – *Cebus*:Posterior	0.000	NS

FIGURE 3 Maximum principal strain (ε) magnitudes depicted for all experimental animals, gage locations, masticatory cycle types, and food item types-Prediction 1.2. Specimens with the designation *G* are gracile in phenotype. Specimens with the designation *R* are robust in phenotype.
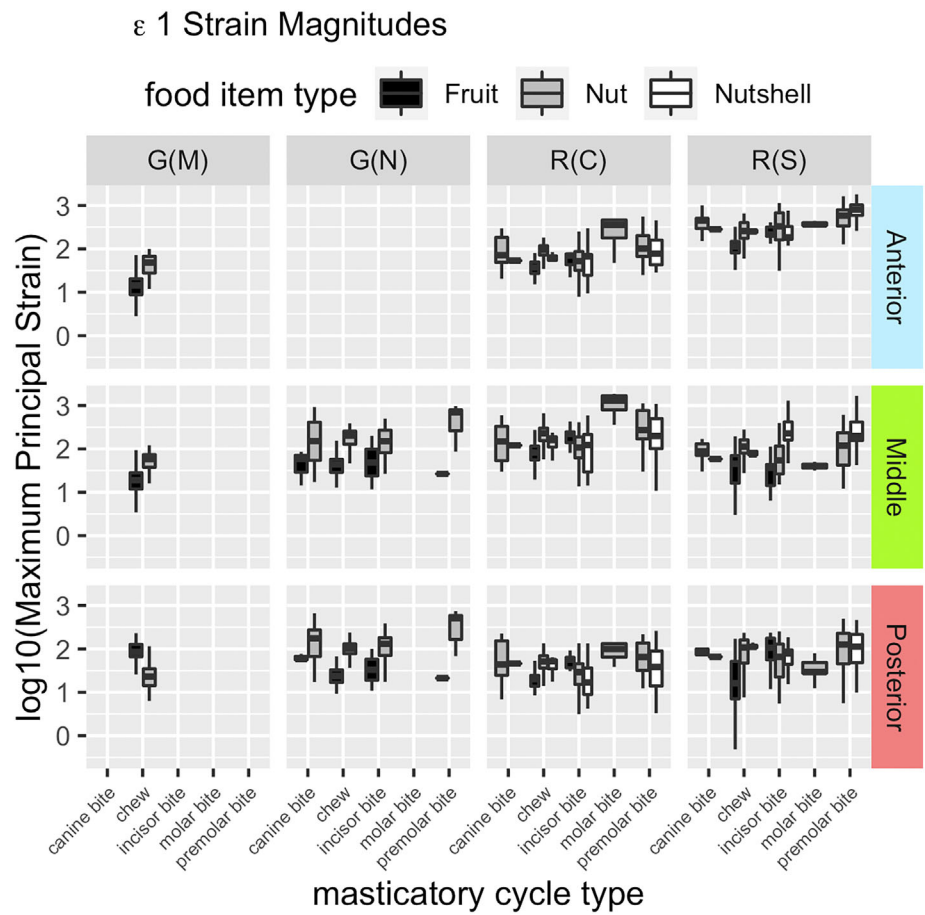

TABLE 4 Results of fixed effects ANOVAs-Prediction 1.2.

		Sum of squares	Mean square	NumDF	DenDF	F value	Pr(>F)
ε_1 magnitude	gage site	323.20	161.60	2	9190.15	1277.03	**<0.0001**
	cycle type	32.63	8.16	4	9182.55	64.46	**<0.0001**
	bite side	0.43	0.43	1	9192.12	3.41	NS
	cranial phenotype	2.16	2.16	1	3.58	17.05	**<0.05**
	sex	3.19	3.19	1	3.56	25.20	**<0.01**
ε_2 magnitude	gage site	68.68	34.34	2	9137.13	209.75	**<0.0001**
	cycle type	37.41	9.35	4	7955.08	57.14	**<0.0001**
	bite side	14.57	14.57	1	8943.77	88.98	**<0.0001**
	cranial phenotype	10.30	10.30	1	17.28	62.95	**<0.0001**
	sex	14.23	14.23	1	16.43	86.95	**<0.0001**
Strain mode	gage site	167.39	83.70	2	9122.22	871.69	**<0.0001**
	cycle type	12.33	3.08	4	8370.40	32.10	**<0.0001**
	bite side	20.54	20.54	1	9125.94	213.90	**<0.0001**
	cranial phenotype	0.23	0.23	1	4.07	2.40	NS
	sex	0.39	0.39	1	4.05	4.02	NS

Note: All bold values represent statistical significance at the correspondingly listed *p*-value that is 0.05 or lower.

maximum principal strains were smaller in male sutures (Table 5; estimate = −0.43; *P* < 0.001). Excluding sex, the effect of cranial phenotypes is dwarfed by all the other effects.

Gage site also significantly affected strain mode (Table 6, *P* < 0.0001; Figure 4; summary statistics are in Supplementary Data Table 6). Higher strain mode values (more tensile strains) were

TABLE 5 Linear mixed model statistics-Prediction 1.2.

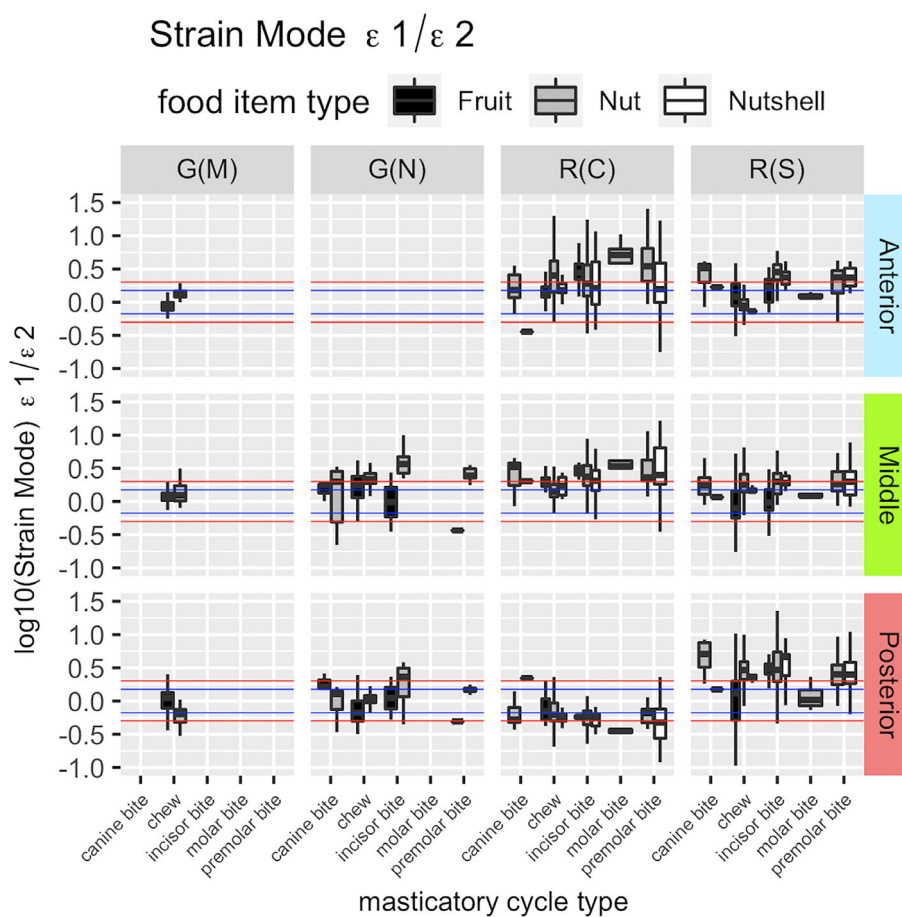| Predictors	Log10 (ε_1)			Log10 (ε_2)			Log10 ($\varepsilon_1/\varepsilon_2$)		
	Estimates	CI	p	Estimates	CI	p	Estimates	CI	p
(Intercept)	2.10	1.85–2.35	**<0.001**	1.72	1.55–1.88	**<0.001**	0.38	0.26–0.51	**<0.001**
gage site [Middle]	0.09	0.07–0.11	**<0.001**	0.17	0.15–0.19	**<0.001**	−0.09	−0.10−−0.07	**<0.001**
gage site [Posterior]	−0.34	−0.36−−0.32	**<0.001**	−0.02	−0.04–0.01	0.158	−0.32	−0.34−−0.31	**<0.001**
cycle type [chew]	−0.00	−0.05–0.05	0.995	0.04	−0.02–0.10	0.187	−0.04	−0.09–0.00	0.061
cycle type [incisor bite]	−0.15	−0.20−−0.09	**<0.001**	−0.18	−0.24−−0.11	**<0.001**	0.05	0.00–0.10	**0.035**
cycle type [molar bite]	−0.09	−0.19–0.01	0.084	0.05	−0.07–0.17	0.386	−0.14	−0.23−−0.05	**0.002**
cycle type [premolar bite]	0.16	0.10–0.22	**<0.001**	0.09	0.02–0.16	**0.012**	0.09	0.04–0.14	**0.001**
CHEW Side [R]	−0.01	−0.03–0.00	0.065	0.08	0.06–0.10	**<0.001**	−0.10	−0.11−−0.08	**<0.001**
Cranial Phenotype [R]	0.30	0.16–0.45	**<0.001**	0.22	0.16–0.27	**<0.001**	0.09	−0.02–0.21	0.122
sex [M]	−0.43	−0.59−−0.26	**<0.001**	−0.29	−0.35−−0.23	**<0.001**	−0.14	−0.27−−0.00	**0.045**
Random effects									
σ^2	0.13			0.16			0.10		
τ_{00}	0.00 individual			0.00 individual			0.00 individual		
	0.04 Food.Item.Type			0.02 Food.Item.Type			0.00 Food.Item.Type		
ICC	0.24			0.10			0.06		
N	3 Food.Item.Type			3 Food.Item.Type			3 Food.Item.Type		
	4 individual			4 individual			4 individual		
Observations	9196			9142			9128		
Marginal R^2/Conditional R^2	0.207/0.395			0.080/0.171			0.184/0.232		
AIC	7142.355			9443.579			4563.832		

Note: All bold values represent statistical significance at the correspondingly listed p-value that is 0.05 or lower.

TABLE 6 Results of random effects ANOVAs-Prediction 1.2.

		npar	logLik	AIC	LRT	Df	Pr(>Chisq)
ε_1 magnitude		13	−3558.18	7142.35			
	food item type	12	−4049.42	8122.84	982.48	1	**<0.0001**
	individual	12	−3659.98	7343.95	203.60	1	**<0.0001**
ε_2 magnitude		13	−4708.79	9443.58			
	food item type	12	−4871.23	9766.47	324.89	1	**<0.0001**
	individual	12	−4709.99	9443.97	2.40	1	NS
Strain Mode		13	−2268.92	4563.83			
	food item type	12	−2358.34	4740.69	178.86	1	**<0.0001**
	individual	12	−2357.3648	4738.73	176.90	1	**<0.0001**

Note: All bold values represent statistical significance at the correspondingly listed p-value that is 0.05 or lower.

recorded at the anterior compared to the middle and posterior gage sites (grand mean anterior vs. middle vs. posterior = 0.298 vs. 0.223 vs. −0.016). Strain mode was also affected by bite side (F-ratio = 214.21; P < 0.0001; Table 6), with left and right side chewing being modestly (but significantly) different from one another. Strain mode was also affected by cycle type (F-ratio = 32.09; P < 0.0001; Table 6): premolar biting was associated with the highest strain mode values, that is, the suture is loaded more in tension. Strain

modes during chewing, canine biting, and molar biting were lower than during incisor biting. Cranial phenotype and sex are either not at all significant, or only marginally so (Table 5; P = 0.122 and P = 0.045 respectively). Strain mode was also significantly affected by food type and individual, with inter-individual effects being stronger than food type (Table 6); the two robust individuals generated more tensile strain than the gracile individuals (LRT = 239.0; P < 0.0001; Table 6), and feeding on nuts and nutshells produced higher (more tensile)

FIGURE 4 Strain modes (the ratio of maximum principal strain to minimum principal strain: $\varepsilon_1/\varepsilon_2$) depicted for all experimental animals, gage locations, masticatory cycle types, and food item types-Prediction 1.2. Values above +0.301 (upper red line) represent high tension, values below −0.301 (lower red line) represent high compression, and values between +0.176 and −0.176 (blue lines) represent shear. Specimens with the designation *G* are gracile in phenotype. Specimens with the designation *R* are robust in phenotype.

strain modes than feeding on tough foods (LRT = 183.9; *P* < 0.0001; Table 6 and Figure 4).

Strain orientation is illustrated in Figure 5 divided across individual, bite side, and cycle type; vertical is the orientation of sagittal planes. The summary and inferential statistics of these cycle type groupings reveal that mean directions also have strong mean resultant lengths and all are significantly non-uniform (reject the null hypothesis of the Rao Spacing Test of Uniformity, summary statistics are in Supplementary Data Table 7). Strain orientation was most strongly affected by bite side, especially in animals G(M) and R(C) (Table 6; *P* < 0.0001). The next strongest effect was gage site (*P* < 0.0001), with strain orientations at the middle location being significantly different from those at the anterior and posterior sites. Cycle type had a marginally significant effect on strain orientation (Table 6; *P* < 0.01). The sagittal suture of G(M) experienced more laterally directed strain orientations at all gage locations, the two robust individuals showed peak strain orientations that were less uniform and less laterally directed at the anterior and middle gage sites, and the very robust individual S had laterally directed strain orientations at the posterior gage site (Figure 5).

The circular mixed effects model indicated that strain orientation is best explained by including chew side, gage location, cycle type, and cranial phenotype into the model (Table 7; DIC = 1433.9). The posterior estimates of the circular means of each group are compared to determine whether any of the 30 combinations of effect levels are significantly different. Groups are said to be significantly different if their 95% lower bound and upper bound intervals do not overlap. From the 95% confidence limits (Table 7) and the plot of these boundaries (Figure 6), it is evident that mostly chews belonging to the gracile phenotype, posterior gage location, biting cycle type, and on mostly the left side are significantly different from all other groupings in their strain orientations. This supports Prediction 1.2, the direction of strains in the posterior region of the sagittal suture are significantly different from those in the anterior and middle regions.

3.3 | Prediction 2.1: Posterior temporalis activity better explains the variance in sagittal suture strain regime during feeding than the anterior temporalis

We first tested for a shared pattern of temporalis activity across individuals. Figure 7 shows the relative timing of muscle activity in the temporalis muscles and superficial masseters of one individual (G(M)) during chewing. Table 8 summarizes the relative timing of peak amplitude for all animals and both chew sides, as well as the ranked order of peak amplitude relative to WSM (working side masseter). Despite both inter-chew side and inter-individual variation, several patterns are consistently seen: the working side posterior temporalis (WPT) always peaks before working middle temporalis (WMT), before working anterior temporalis (WAT; except for animal N), and before
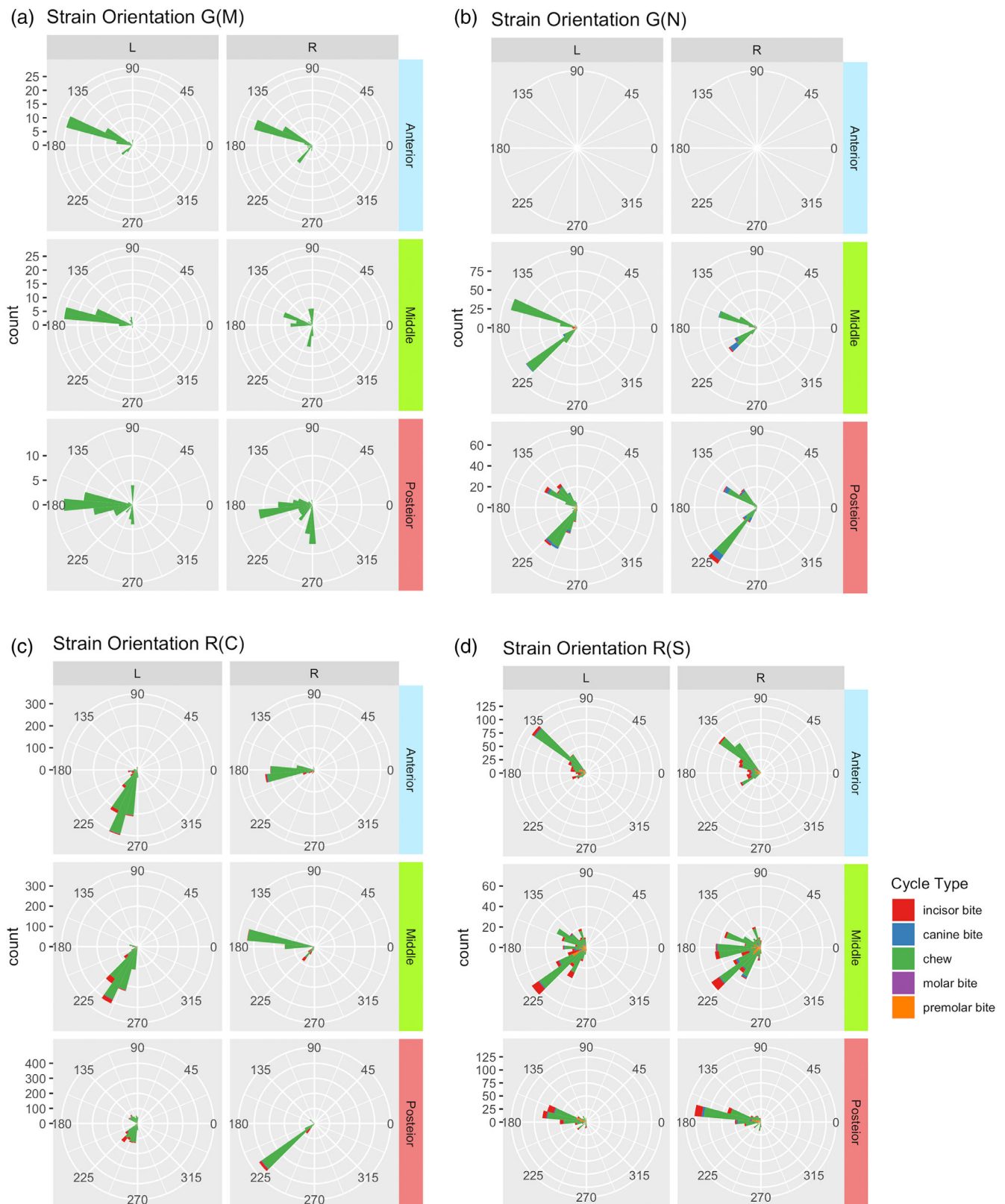
12 | **WILEY** | AMERICAN JOURNAL OF BIOLOGICAL ANTHROPOLOGY
The Official Journal of the American Association of Biological Anthropologists

BYRON ET AL.

FIGURE 5 Circular histograms depicted for all experimental animals, gage locations, and masticatory cycle types-Prediction 1.2. The orientation of the maximum principal strain relative to the mid-sagittal plane was calculated, with 0° being perpendicular to the sagittal plane of the cranium. All left and right chews have been normalized to this axis. Specimens with the designation *G* are gracile in phenotype. Specimens with the designation *R* are robust in phenotype.

TABLE 7 Results bayesian mixed effects model building-Prediction 1.2.

	Individual (or intercept)	Side	Side + location	Side + location + cycle type	Side + location + cycle type + cranial phenotype
DIC	16064.9	15915.0	13385.3	13373.0	13334.7
WAIC	16067.1	15918.1	13391.9	13383.3	13383.5

	95% Confidence Intervals	
Cat_Fac_Groups	**Lower Boundary**	**Upper Boundary**
Left, Anterior, Canine Bite, Gracile	30.7	116.1
Right, Anterior, Canine Bite, Gracile	25.8	143.3
Left, Posterior, Canine Bite, Gracile	**142.4**	**359.9***
Left, Middle, Canine Bite, Gracile	21.9	144.6
Left, Anterior, Chew, Gracile	26.3	113.3
Left, Anterior, Incisor Bite, Gracile	21.9	104.1
Left, Anterior, Molar Bite, Gracile	21.8	102.4
Left, Anterior, Premolar Bite, Gracile	22.0	105.5
Left, Anterior, Canine Bite, Robust	18.1	120.3
Right, Posterior, Canine Bite, Gracile	**175.6**	**292.7***
Right, Middle, Canine Bite, Gracile	7.4	178.4
Right, Anterior, Chew, Gracile	20.1	142.7
Right, Anterior, Incisor Bite, Gracile	12.8	133.8
Right, Anterior, Molar Bite, Gracile	13.1	127.7
Right, Anterior, Premolar Bite, Gracile	17.0	136.7
Right, Anterior, Canine Bite, Robust	7.6	157.1
Left, Posterior, Chew, Gracile	**167.1**	**356.3***
Left, Posterior, Incisor Bite, Gracile	174.9	3.3
Left, Posterior, Molar Bite, Gracile	120.3	26.6
Left, Posterior, Premolar Bite, Gracile	**163.6**	**358.7***
Left, Posterior, Canine Bite, Robust	**−177.9**	**−23.2***
Left, Middle, Chew, Gracile	14.7	143.3
Left, Middle, Incisor Bite, Gracile	8.1	135.3
Left, Middle, Molar Bite, Gracile	11.6	131.3
Left, Middle, Premolar Bite, Gracile	13.2	138.9
Left, Middle, Canine Bite, Robust	7.4	165.7
Left, Anterior, Chew, Robust	15.3	120.0
Left, Anterior, Incisor Bite, Robust	7.0	103.9
Left, Anterior, Molar Bite, Robust	12.6	106.2
Right, Posterior, Canine Bite, Gracile	12.9	111.9

*A bold value with asterisk denotes significance, $p < 0.05$.

balancing anterior (BAT) and posterior temporalis (BPT). BPT always peaks after BAT and, with the exception of animal R(C), is last out of all the muscles (Table 8). Tests for difference in rank order reveal that: WPT peaks significantly earlier than BMT ($P < 0.05$), BPT ($P < 0.01$), WMT ($P < 0.01$), and WSM ($P < 0.05$); WAT peaks significantly earlier than BPT ($P < 0.05$); and BPT peaks significantly later than BAT ($P < 0.01$) (Table 9, Figure 8).

The multiple regression analyses produced a statistically significant model for each of the strain gage locations as listed in Table 10 (Anterior $R^2 = 12\%$, $F = 61.15$, $P < 0.0001$; Middle $R^2 = 62\%$, $F = 730.76$, $P < 0.0001$; Posterior $R^2 = 21\%$, $F = 119.43$, $P < 0.0001$). Table 11 lists the multiple regression model coefficients. EMG activity in the middle and posterior parts of the muscle is correlated with strain at the middle gage (i.e., significant positive coefficients of 14.2, 15.7, 7.4, 14.3, $P < 0.0001$); posterior temporalis EMG amplitudes best explained strain at the anterior and posterior gage sites (i.e., significant positive coefficients of 19.1, 12.4, $P < 0.0001$ and a significant negative coefficient of −10.4, $P < 0.0001$).
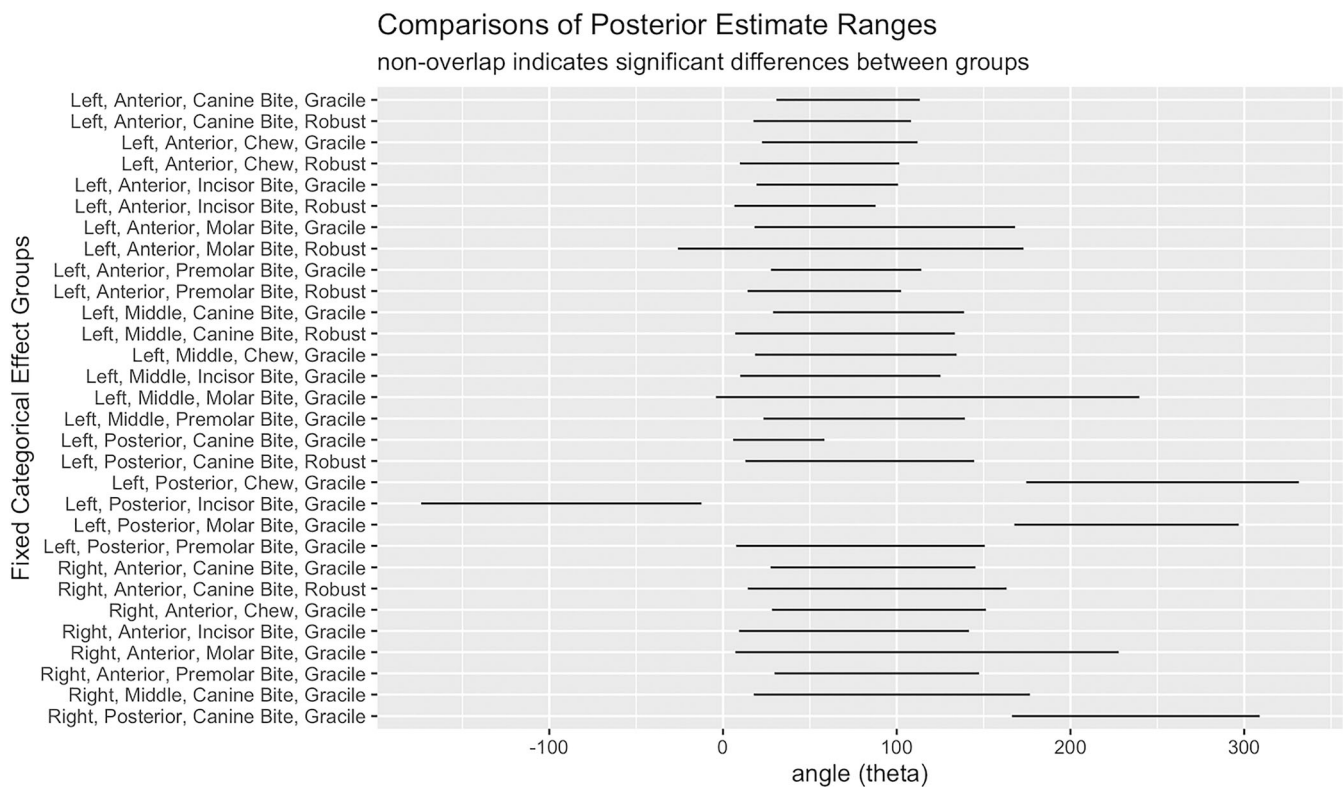
Comparisons of Posterior Estimate Ranges
non-overlap indicates significant differences between groups

FIGURE 6 Plot depicting 95% confidence intervals of the Bayesian Mixed Effects Model comparing all combinations of effects levels-Prediction 1.2. Non-overlapping intervals indicates significantly different groups.

3.4 | Prediction 2.2: Chewing side-related variation in relative timing of working and balancing posterior temporalis activity is associated with side-related variation in strain regime

We tested whether strain regimes vary more across chewing sides than across individuals. The Beta Square and Ginizi methods for proportioning R^2 of each model to EMG location also reveal that strain at the middle gage location is best explained by all aspects of temporalis function (Figure 9). The anterior gage location appears to be better explained by right side temporalis activity. The posterior gage location strain is best explained by left side posterior temporalis activity.

4 | DISCUSSION

Current understanding of sutural form-function relationships is complicated by scattered taxon sampling (*Polypterus*, *Caiman*, *Sus*, *Macaca*, *Mus*, *Sapajus*, and other rodents) and a lack of in vivo data from an appropriately broad range of natural feeding behaviors. This study tested hypotheses about form-function relationships of cranial sutures by studying the strain regime in the sagittal sutures of gracile and robust capuchin primates during feeding on diverse foods and employing different behaviors. By documenting sutural strain regime during feeding on a range of foods, we hoped to

illuminate the biomechanical factors affecting sutural shape in other vertebrates.

The four individuals available for study did not constitute an ideal sample. Their precise species membership is unknown, and the sex balance was uneven (three males and one female) which also impacts the cranial phenotype variable. Experimentally, fewer useful gape cycles were collected on the gracile specimens and the robust specimens included a greater diversity of cycle types and food items (Figures 3–5). This is a limitation of the existing data set. However, the variation in craniofacial robusticity and sutural morphology in our sample was representative of the major axes of variation in museum samples of wild populations (Figure 1): our laboratory sample resembles museum specimens in that the more robust individuals have more sinuous sagittal sutures than the gracile individuals. Additionally, the museum and laboratory samples provide support for Prediction 1.1, in that greater suture sinuosity, amplitude, and spacing are found in the anterior region of the sagittal suture and in robust capuchin morphotypes. This corresponds to regions with the largest maximum principal strain. That is, increased anterior and middle suture complexity metrics are linked to increased anterior and middle sutural strain regimes, and these are generally decreased in the posterior region (see Figure 4 R(C)-Anterior-Premolar Bite-Nutshell).

Gage location along the suture had a strongly significant impact on strain magnitude, strain mode, and strain orientation (Prediction 1.1). The highest strain magnitudes were recorded in the middle of
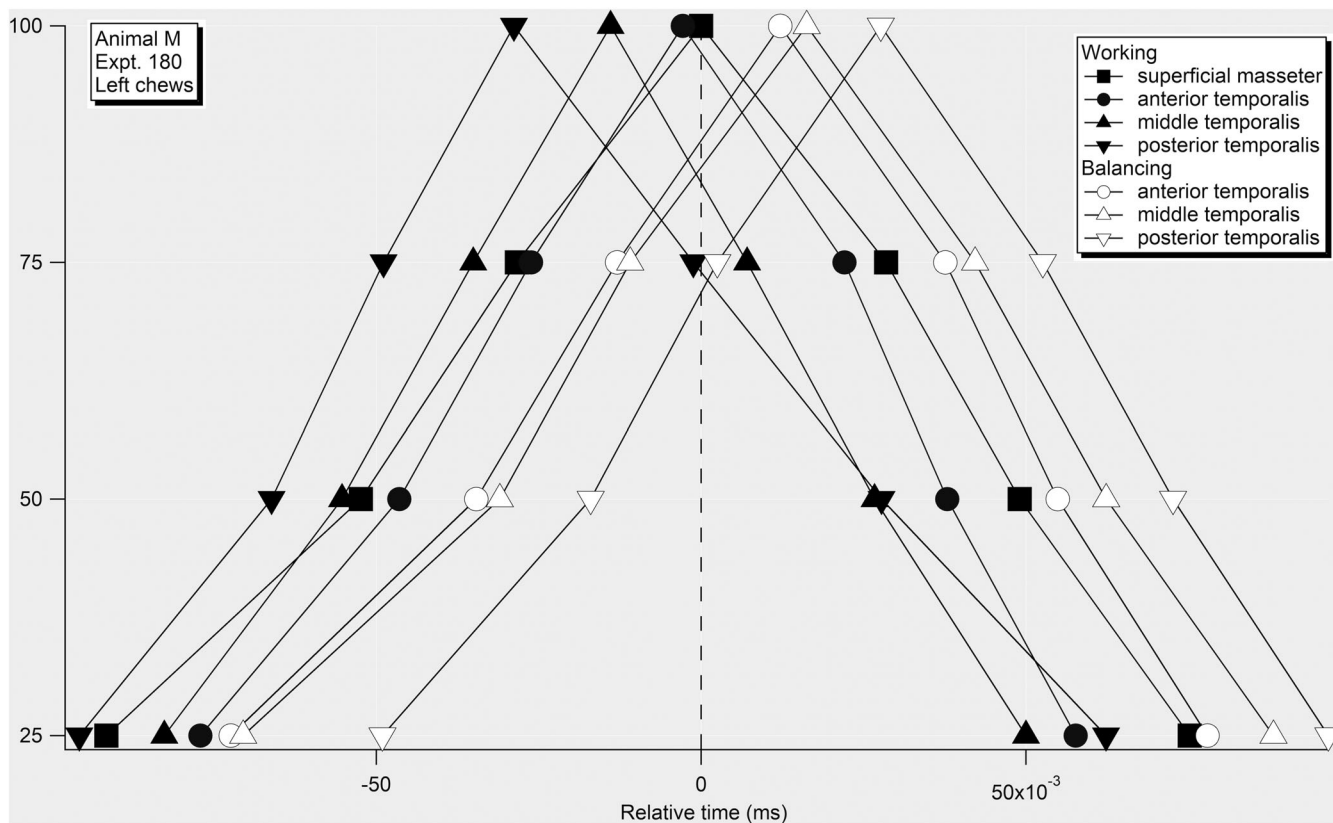
FIGURE 7 Representative plot of relative timing of muscle activity in working and balancing side temporalis muscles during chewing-Prediction 2.1 and 2.2. Points are mean timing of 25, 50, 75, and 100% of peak activity relative to peak activity in working side superficial masseter (WSM). Gracile animal M, experiment 180, left chews.

TABLE 8 Relative timing of peak activity in working and balancing temporalis muscles during chewing-Prediction 2.1 and 2.2.

Animal	Robust (R) Gracile (G)	Chew side	Before WSM	After BSM
M	G	right	WPT	WMT, WAT, BMT, BAT, BPT
M	G	left	WPT, WMT, WAT	BAT, BMT, BPT
N	G	right	WAT/BAT/WPT, WMT, BMT	BPT
N	G	left	WAT/WPT, BAT	BMT, WMT, BPT
C	R	right	WPT, BMT, BAT, BPT	WAT, WMT
C	R	left	BMT, BAT, WPT	BPT, WAT, WMT
S	R	right	WPT	WAT, BMT, BPT
S	R	left	BAT, WPT	WMT, BPT

Abbreviations: BAT, balancing anterior temporalis; BMT, balancing middle temporalis; BPT, balancing posterior temporalis; LATP, Left Right anterior temporalis; LMTP, Left middle temporalis; LPTP, Left posterior temporalis; RATP, Right anterior temporalis; RMTP, Right middle temporalis; RPTP, Right posterior temporalis; WAT, working anterior temporalis; WMT, working middle temporalis; WPT, working side posterior temporalis; WSM, working side masseter.

the suture and the lowest in the posterior suture, near lambda. Unlike pigs, in which the posterior sagittal suture was tensed and the anterior sagittal suture was compressed (Herring & Teng, 2000), strain mode varied along the suture such that posterior gage locations had lower values than the anterior and middle locations. Strain mode values in some cases are compression or types of strain mode nearly ≤ -0.301 (see Figure 4; R(C)-Posterior-Premolar Bite-Nut-shell), indicating a less tensional environment along the more

posterior aspects of the sagittal suture. Indeed, strain mode is more strongly affected by gage location than by bite side or individual. Strain orientation also varied along the suture, although the effects were small compared with variation between individuals and bite sides and inconsistent across animals. The orientation of strains at the posterior gage location were significantly different from those in the middle and anterior locations. All these results are consistent with Prediction 1.2; strain regimes varied significantly along the

16 | **WILEY**—AMERICAN JOURNAL OF BIOLOGICAL ANTHROPOLOGY
The Official Journal of the American Association of Biological Anthropologists

BYRON ET AL.

TABLE 9 Test of significance of differences in rank order-Prediction 2.1 and 2.2.

LME ANOVA results	numDF	denDF	F-value	p-value
(Intercept)	1	38	270.63626	**<0.0001**
Muscle	6	38	5.89171	**<0.001**
LME Tukey contrasts	Estimate Std.	Error	z value	Pr(>|z|)
BMT-BAT	1	0.809	1.236	NS
BPT-BAT	2.875	0.7833	3.67	**<0.01**
WAT-BAT	0.2857	0.809	0.353	NS
WMT-BAT	1.7143	0.809	2.119	NS
WPT-BAT	−1.625	0.7833	−2.075	NS
WSM-BAT	0.75	0.7833	0.958	NS
BPT-BMT	1.875	0.7833	2.394	NS
WAT-BMT	−0.7143	0.809	−0.883	NS
WMT-BMT	0.7143	0.809	0.883	NS
WPT-BMT	−2.625	0.7833	−3.351	**<0.05**
WSM-BMT	−0.25	0.7833	−0.319	NS
WAT-BPT	−2.5893	0.7833	−3.306	**<0.05**
WMT-BPT	−1.1607	0.7833	−1.482	NS
WPT-BPT	−4.5	0.7567	−5.947	**<0.001**
WSM-BPT	−2.125	0.7567	−2.808	NS
WMT-WAT	1.4286	0.809	1.766	NS
WPT-WAT	−1.9107	0.7833	−2.439	NS
WSM-WAT	0.4643	0.7833	0.593	NS
WPT-WMT	−3.3393	0.7833	−4.263	**<0.001**
WSM-WMT	−0.9643	0.7833	−1.231	NS
WSM-WPT	2.375	0.7567	3.139	**<0.05**

Note: All bold values represent statistical significance at the correspondingly listed p-value that is 0.05 or lower.

FIGURE 8 Rank order of peak muscle activity in working (W) and balancing (B) anterior (AT), middle (MT) and posterior (PT) temporalis muscles-Prediction 2.1 and 2.2. See Table 8 for statistical details. *, timing significantly different at $P < 0.05$; **, timing significantly different at $P < 0.01$; ***, timing significantly different at $P < 0.001$.

Macaca, *Papio* and *Aotus*) reveal that the calvarial bones are routinely twisted during mastication (Bourbon, 1982; Herring & Teng, 2000; Hylander et al., 1991; Lieberman et al., 2004; Ravosa et al., 2000; Ross et al., 2009; Ross et al., 2011; Ross & Hylander, 1996), making it unlikely that the sagittal sutures of our capuchins are under pure laterally directed tensile strain. Indeed, only in one individual (G(M)) were maximum principal strains directed mostly laterally a majority of the time at all three gage sites, and even in this individual strain orientation varied with chew side (Figure 5). As noted, experimental challenges led to this specimen's incompleteness of data across all cycle and food types. It might be true that simple chewing strains from fruits and nuts can be mostly lateral in direction at all gage sites, but these would likely change significantly as different gape cycle types are employed. Simplistic ideas of laterally directed tension in sagittal sutures during feeding do not describe the strain regime in capuchins. If calvarial bone and sutural strain data of the mammals listed above are indicative of the strain regimes in the sutures connecting them, simplistic models of sutural strain do not apply in these species either.

Behrents et al. (1978) recorded strain magnitudes of 70 με (microstrain) from the parietal bones and 180 με across the suture.[1] Congruent with these data, Bourbon (1982) reported sagittal suture strains between 87–116 με during single muscle stimulation and 183 με during chewing. Smith and Hylander (1985) documented tensile strains of up to 14,000 με, compared with several hundred microstrain from rosette gages on adjacent bones. Our results are closer to the data reported by Behrents et al. (1978) and Bourbon (1982). Sagittal suture strains measured in our gracile specimens were around 200 με, and less for most foods at all three strain gage locations. In our most

sagittal suture, with anterior and middle gage locations showing higher strain magnitudes and more similar strain orientations than with the posterior location which differs most substantially. These results support the hypothesis that cranial suture waveform growth is affected by feeding strains—greater sinuosity, amplitude, and spacing in the anterior and middle sagittal suture regions is linked to higher strain magnitudes and modes.

Prediction 1.2 implies that strain regimes vary with location along the suture, with biting side, with feeding behavior, and with food material properties, and that this includes strain orientation data. These predictions were borne out to various degrees. An assumption of purely laterally directed strain at the sagittal suture during feeding is unwarranted. Muscle stimulation studies in macaques and pigs have shown that temporalis activation puts the sagittal suture under laterally directed tension (Behrents et al., 1978; Herring & Teng, 2000), but single element strain gages only give information on strains along the axis of the gage, they do not allow inferences about twisting or shear that might be revealed by principal strain orientation data. Strain data from pigs and various primates (*Eulemur*, *Varecia*, *Otolemur*,
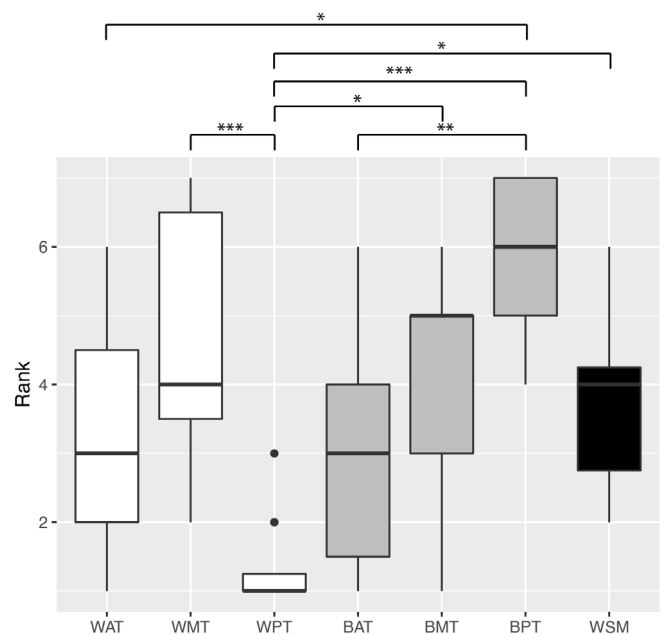
TABLE 10 Multiple regression summary statistics-Prediction 2.1 and 2.2.

gage	r.squared	adj.r.squared	Sigma	Statistic	p.value	df	logLik	AIC	BIC	Deviance	df.residual
Anterior	0.12	0.12	0.37	61.15	**<0.0001**	7	−1128.57	2273.15	2320.49	365.79	2740
Middle	0.62	0.61	0.26	730.76	**<0.0001**	7	−179.55	375.10	422.44	183.30	2740
Posterior	0.21	0.21	0.35	119.43	**<0.0001**	7	−977.94	1971.89	2019.23	327.80	2740

Note: All bold values represent statistical significance at the correspondingly listed *p*-value that is 0.05 or lower.

TABLE 11 Multiple regression coefficient statistics-Prediction 2.1 and 2.2.

Model	Term	Estimate	Std.error	Statistic	p-value
Anterior	(Intercept)	2.0309	0.0129	157.1	**<0.0001**
Anterior	LATP	0.0009	0.0006	1.4	NS
Anterior	LMTP	−0.0007	0.0006	−1.1	NS
Anterior	LPTP	0.0048	0.0006	7.9	**<0.0001**
Anterior	RATP	−0.0103	0.0011	−9.8	**<0.0001**
Anterior	RMTP	−0.0071	0.0007	−10.1	**<0.0001**
Anterior	RPTP	0.0062	0.0004	14.2	**<0.0001**
Middle	(Intercept)	1.6590	0.0091	181.3	**<0.0001**
Middle	LATP	−0.0032	0.0005	−7.1	**<0.0001**
Middle	LMTP	0.0064	0.0005	14.2	**<0.0001**
Middle	LPTP	0.0067	0.0004	15.7	**<0.0001**
Middle	RATP	−0.0070	0.0007	−9.5	**<0.0001**
Middle	RMTP	0.0036	0.0005	7.4	**<0.0001**
Middle	RPTP	0.0044	0.0003	14.3	**<0.0001**
Posterior	(Intercept)	1.4713	0.0122	120.2	**<0.0001**
Posterior	LATP	−0.0011	0.0006	−1.9	NS
Posterior	LMTP	−0.0001	0.0006	−0.2	NS
Posterior	LPTP	0.0109	0.0006	19.1	**<0.0001**
Posterior	RATP	−0.0003	0.0010	−0.3	NS
Posterior	RMTP	−0.0069	0.0007	−10.4	**<0.0001**
Posterior	RPTP	0.0051	0.0004	12.4	**<0.0001**

Note: All bold values represent statistical significance at the correspondingly listed *p*-value that is 0.05 or lower.

robust experimental animal when eating nuts and nutshells, strains increased to 500 με, and in some cases exceeded >1000 με. On average across all >9000 biting or chewing cycles, food type effects on maximum principal strains are less than those effects caused by other independent variables such as gage site, gape cycle types, sex, and cranial phenotype. Conversely, food type effects on maximum principal strain are greater than biting side and individual effects. In other related analyses (Ross et al., 2016) food item effects are also not as significant as effects caused by gape cycle type and biting side. Our new data on sutural strains are congruent with these earlier results, and with the prediction that gape cycle type is responsible for more variation in a strain regime than food type. The effect of sex on strain magnitude data indicates that male sutures experienced significantly lower maximum and minimum principal strains (Table 5; estimates = −0.43 and −0.29 respectively, P < 0.0001). In particular, our data suggest that if males and females are eating the same foods and generating the same forces (as supported by behavioral studies,

e.g., Laird, Wright, et al., 2020; Wright, 2005), this may be associated with higher strains in a smaller animal. However, because we only sampled one female individual, the influence of sex on strain in capuchins requires future research.

Our previous work with some of the animals used in this study revealed that variation in feeding behavior had a significant effect on strain regimes in the mandible (Ross et al., 2016), so we expected to see variation in sagittal suture strain regime with cycle type. Cycle type and food type were more important drivers of strain magnitude (ε_1 and ε_2) than of strain mode. Notably, when the most robust capuchin processed obdurate foods, such as Brazil nuts, hazelnuts, and walnuts, the anterior suture region experienced significantly higher strain magnitudes than middle and posterior suture regions, and higher strains than in the other capuchins. Sutural strain, especially in the anterior region, is significantly impacted by feeding behaviors related to gape cycle and food type, especially nuts and nutshells. Strain magnitudes were higher during

18 | WILEY—AMERICAN JOURNAL OF BIOLOGICAL ANTHROPOLOGY
The Official Journal of the American Association of Biological Anthropologists
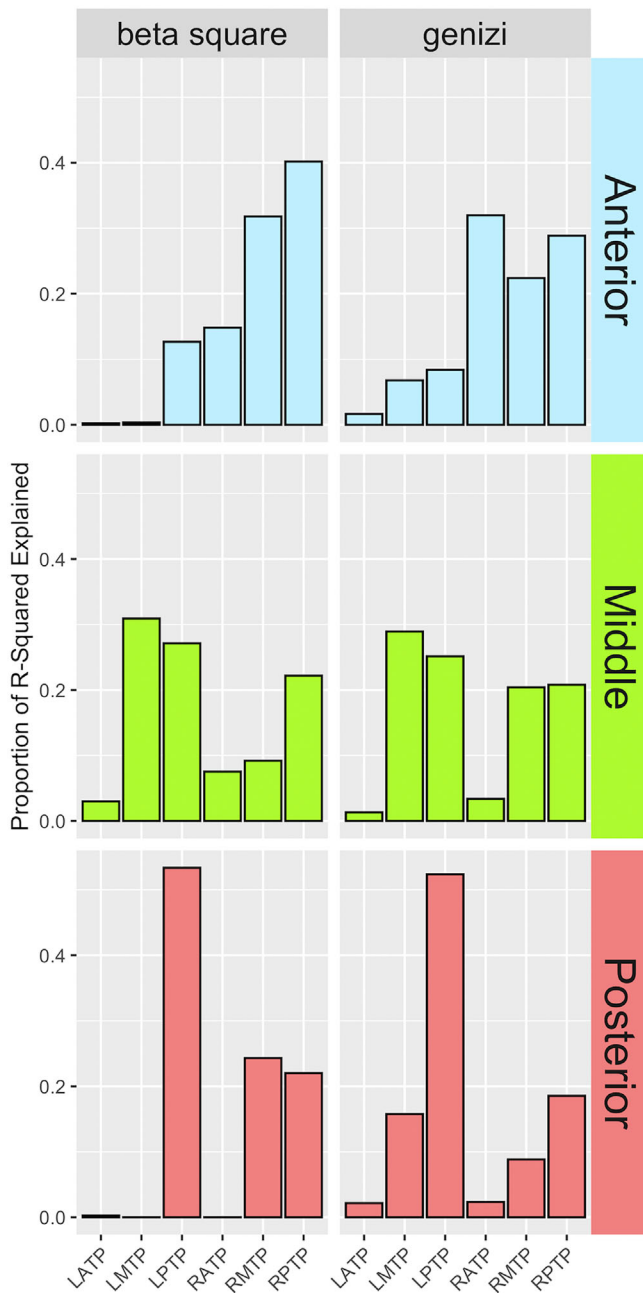
BYRON ET AL.

FIGURE 9 Comparison of multiple regression models predicting maximum principal strain amplitude at each gage location using all six left and right temporalis EMG locations-Prediction 2.1 and 2.2. Beta square and Genizi represent different methods for calculating the proportion of R^2 explained by each EMG location.

Rafferty & Herring, 1999; Smith & Hylander, 1985; Sun et al., 2002; Sun et al., 2004). We recognize that non-masticatory muscles may also play a significant role in certain ingestive behaviors. For example, splenius capitis, and other extensors of the neck may help to stabilize the back of the cranium during forceful biting. These data are beyond the scope of this present study and so are left unaddressed.

Our data also provide support for Prediction 2.1 that posterior temporalis EMG effort has a stronger influence than anterior temporalis effort on sagittal suture strain regime. This was true for both left and right temporalis and both anterior and posterior gage locations. Posterior gage strain is driven by both right and left posterior temporalis, whereas strain at the anterior gage was driven mainly by right side posterior temporalis. Strain at the middle gage was driven equally by middle and posterior temporalis activity from both right and left sides. These results support the hypothesis that the posterior temporalis plays a greater role than the anterior temporalis in sagittal suture strain regimes. This probably reflects the closer proximity of the posterior temporalis to the sagittal suture in capuchin primates and its greater timing asymmetry than seen in other bilateral masticatory muscles. It is worth noting that gape cycles begin with working side posterior temporalis activity and they end with balancing side posterior temporalis activity (Figure 8) resulting in little to no instantaneous time overlap between working and balancing side muscle action.

Our data did reveal significant inter-individual effects on sagittal suture strain regime. Assuming gage locations—anterior, middle, posterior—are homologous across the four animals, two possible sources of inter-individual effects warrant discussion: variation in local strain environments, perhaps associated with sutural morphology, and inter-individual variation in muscle recruitment patterns. It is possible that variation in the micro-anatomy of the suture between individuals (i.e., small changes in interdigitation) may have a significant but localized effect on the strain pattern at the suture. The path of each suture is distinctive and individual, and this might influence local strain with respect to potential regions of stress concentration. It could even be the case that suture morphology is an emergent property of the complex micromechanical environment of the suture connective tissue fibroblast cells and their extracellular matrix. Suture waveform increases sutural volume and this might mitigate strain at some local level not being accounted for here.

It is also possible that inter-individual variation in sutural strain might be related to individual variation in muscle recruitment (Prediction 2.2). For example, Animal R(C) exhibits the largest consistent differences in strain orientation with chew side (Figure 5) and differs from the other animals in showing consistent differences in relative timing of middle and posterior temporalis muscles, the muscles closest to the sagittal suture (Tables 8–10). In Animal R(C) the balancing side middle temporalis (BMT) is always active early in the sequence and the WMT is always active last, regardless of chew side, and the BPT shows relatively early peak activity. Exactly how these relative timing variables might be related to sagittal suture strain regimes is opaque and our results argue against a strong relationship

ingestive behaviors (specifically premolar biting) than chewing. If sagittal suture morphology reflects strain environment, it most likely is related to variation in feeding behavior, especially ingestive behaviors, than diet per se (Behrents et al., 1978; Herring et al., 1993; Herring & Mucci, 1991; Herring & Teng, 2000; Hubbard et al., 1971; Oudhof & van Doorenmaalen, 1983; Persson, 1995; Popowics & Herring, 2007; Rafferty et al., 2003;

WILEY

between muscle recruitment and sagittal suture strain. Cycle type—incisor bite, canine bite, chew—is known to be associated with significant variation in muscle recruitment patterns (Hylander & Johnson, 1985; Ross & Hylander, 2000), but cycle type has minimal influence on strain orientation in the sagittal suture. Our data do show significant effects of bite side on strain orientations, and this might be invoked to support a link between muscle recruitment and strain orientation because chewing side is known to impact muscle recruitment patterns in the temporalis (Hylander & Johnson, 1985; Hylander et al., 2005). However, it seems unlikely that variation in muscle recruitment associated with bite side would be larger than variation associated with cycle type (Vinyard et al., 2008). Instead, we hypothesize that variation in bite side may be affecting sagittal suture strain regime forces acting at the temporomandibular joint (TMJ). Theoretical analyses and experimental data from macaques suggest that TMJ reaction forces can be high and vary significantly with bite side (Panagiotopoulou et al., 2020). The possibility that TMJ reaction forces might affect sagittal suture strain regimes warrants further study.

Sutures are important areas that modulate cranial growth (Opperman, 2000) while also transducing mechanical signals that help shape craniofacial development (Roth et al., 2022). In the calvaria, this expansion accommodates a rapidly growing brain early in life, but by the time individuals reach adulthood brain growth has ceased and masticatory loading continues, and probably is of higher magnitude than at earlier life stages. Depending on the stress concentrations within suture connective tissue, they may begin to grow increasingly complex as a way of maximizing suture volume to protect fragile suture connective tissue (Wang et al., 2010, 2012). We hypothesize that the expansion of the temporalis muscle in robust capuchins, in order to process stress-limited foods, might explain subtle differences in suture morphology observed between gracile and robust capuchins. More broadly across anthropoid primates adapted for feeding system overuse, we suggest differences in sutural strain regimes may be driven by activity of the muscles of the feeding system, warranting future testing in other primates. However, more in-depth analysis will depend on a better understanding of the relationships between local morphology and strain environment in cranial joints, perhaps using finite element modeling approaches.

This study integrates comparative cranial suture data and experimental feeding data for primate taxa with contrasting feeding system adaptations. We found increased morphological variation in the anterior suture, and greater anterior sagittal suture tensional and shear strain during premolar and canine biting on displacement limited foods and with craniofacial robusticity—supporting Hypothesis 1. Our results also suggest that anteroposterior, as well as working and balancing side variation in temporalis activity, are significantly related to sagittal suture strain regime—supporting Hypothesis 2. Specifically, the activation pattern of the posterior region of this important jaw elevator contributes to strains at the posterior region of the sagittal suture while strains in the anterior suture region are explained better by biting side. The combination of these findings supports a model for sagittal suture biomechanics wherein a complex strain regime results from the multivariate nature of anthropoid feeding. Cranial suture complexity also seems to be associated with masticatory system overuse, which will inform models of human and non-human primate feeding biomechanics.

AUTHOR CONTRIBUTIONS

ACKNOWLEDGMENTS

FUNDING INFORMATION

CONFLICT OF INTEREST STATEMENT

The authors declare no conflicts of interest.

DATA AVAILABILITY STATEMENT

The raw data that support the findings of this study are available from the corresponding author upon request. All suture morphology and strain data summary statistics are provided in the supplementary materials. The various coded scripts used to carry out the study are also available on request. These scripts are generally saved in html as Markdown files and can be easily shared and replicated by other R users.

20 WILEY AMERICAN JOURNAL OF BIOLOGICAL ANTHROPOLOGY The Official Journal of the American Association of Biological Anthropologists

BYRON ET AL.

ORCID

Craig Byron https://orcid.org/0000-0001-8673-9196
Jose Iriarte-Diaz https://orcid.org/0000-0003-3566-247X
Qian Wang https://orcid.org/0000-0002-3303-1183
David Strait https://orcid.org/0000-0002-3572-1663
Myra F. Laird https://orcid.org/0000-0002-8636-0407
Callum F. Ross https://orcid.org/0000-0001-7764-761X

ENDNOTE

[1] The text in Behrents et al. states that 700 με was recorded from the parietal bones, but in a later paragraph the report states that 180 με was recorded from the suture and that these values were larger than the parietal strains. We assume that 700 should read 70 με. However, it is possible that comparisons across suture gage studies are complicated by high amounts of inter-experimental differences because of issues with bonding across the suture.

REFERENCES

Agostinelli, C., & Lund, U. (2017). R package circular: Circular statistics (version 0.4-93). https://r-forge.r-project.org/projects/circular/

Anapol, F., & Lee, S. (1994). Morphological adaptation to diet in platyrrhine primates. *American Journal of Physical Anthropology*, 94(2), 239–261 http://www.ncbi.nlm.nih.gov/entrez/query.fcgi?cmd=Retrieve&db=PubMed&dopt=Citation&list_uids=8085615

Bates, D., Mächler, M., Bolker, B., & Walker, S. (2015). Fitting linear mixed-effects models using lme4. *Journal of Statistical Software*, 67(1), 1–48. https://doi.org/10.18637/jss.v067.i01

Behrents, R. G., Carlson, D. S., & Abdelnour, T. (1978). In vivo analysis of bone strain about the sagittal suture in *Macaca mulatta* during masticatory movements. *Journal of Dental Research*, 57(9–10), 904–908 http://www.ncbi.nlm.nih.gov/entrez/query.fcgi?cmd=Retrieve&db=PubMed&dopt=Citation&list_uids=102671

Bourbon, B. M. (1982). *Deformation of cranial sutures during masticatory activity: A strain gage application*. University of Pennsylvania.

Byron, C., Segreti, M., Hawkinson, K., Herman, K., & Patel, S. (2018). Dietary material properties shape cranial suture morphology in the mouse calvarium. *Journal of Anatomy*, 233, 807–813. http://doi.wiley.com/10.1111/joa.12888

Byron, C. D. (2006). Role of the osteoclast in cranial suture waveform patterning. *The Anatomical Record Part A: Discoveries in Molecular, Cellular, and Evolutionary Biology*, 288A(5), 552–563. https://doi.org/10.1002/ar.a.20322

Byron, C. D. (2009). Cranial suture morphology and its relationship to diet in *Cebus*. *Journal of Human Evolution*, 57(6), 649–655. https://doi.org/10.1016/j.jhevol.2008.11.006

Byron, C. D., Borke, J., Yu, J., Pashley, D., Wingard, C. J., & Hamrick, M. (2004). Effects of increased muscle mass on mouse sagittal suture morphology and mechanics. *The Anatomical Record. Part A, Discoveries in Molecular, Cellular, and Evolutionary Biology*, 279(1), 676–684. https://doi.org/10.1002/ar.a.20055

Chai, H. (2020). Determining primates bite force from histological tooth sections. *American Journal of Physical Anthropology*, 171, 683–703.

Cheronet, O., Ash, A., Anders, A., Dani, J., Domboróczki, L., Drozdova, E., Francken, M., Jovanovic, M., Milasinovic, L., Pap, I., Raczky, P., Teschler-Nicola, M., Tvrdý, Z., Wahl, J., Zariņa, G., & Pinhasi, R. (2021). Sagittal suture morphological variation in human archaeological populations. *Anatomical Record*, 304, 2811–2822. https://doi.org/10.1002/ar.24627

Cole, T. (1992). Postnatal heterochrony of the masticatory apparatus in *Cebus apella* and *Cebus albifrons*. *Journal of Human Evolution*, 23, 253–282.

Cremers, J. (2018). Bpnreg: Bayesian projected normal regression models for circular data. https://CRAN.R-project.org/package=bpnreg

Cremers, J., & Klugkist, I. (2018). One direction? A tutorial for circular data analysis using R with examples in cognitive psychology. *Frontiers in Psychology*, 9(OCT), 1–13. https://doi.org/10.3389/fpsyg.2018.02040

Daegling, D. J. (1992). Mandibular morphology and diet in the genus *Cebus*. *International Journal of Primatology*, 13(5), 545–570.

Defler, T. R. (1979a). On the ecology and behavior of *Cebus albifrons* in eastern Columbia. I. Ecology. *Primates*, 20, 475–490.

Defler, T. R. (1979b). On the ecology and behavior of *Cebus albifrons* in eastern Columbia. II. Behavior. *Primates*, 20, 491–502.

Dzialo, C., Wood, S. A., Berthaume, M., Smith, A., Dumont, E. R., Benazzi, S., Weber, G. W., Strait, D. S., & Grosse, I. R. (2014). Functional implications of squamosal suture size in *Paranthropus boisei*. *American Journal of Physical Anthropology*, 153, 260–268. https://doi.org/10.1002/ajpa.22427

Farke, A. A. (2008). Frontal sinuses and head-butting in goats: A finite element analysis. *Journal of Experimental Biology*, 211(19), 3085–3094. https://doi.org/10.1242/jeb.019042

Freese, C. H., Oppenheimer, J. R., & Skopec, A. L. (1981). The capuchin monkeys, genus *Cebus*. In A. F. Coimbra-Filho & R. A. Mittermeier (Eds.), *Ecology and behavior of neotropical primates* (Vol. 1, pp. 331–390). Academia Brasileira de Ciencias.

Genizi, A. (1993). Decomposotion of R^2 in multiple regressions. *Statistica Sinica*, 3, 407–420.

Grömping, U. (2006). Relative importance for linear regression in R: The package relaimpo. *Journal of Statistical Software*, 17, 1–27.

Herring, S. W. (1972). Sutures a tool in functional cranial analysis. *Acta Anatomica*, 83(3), 222–247.

Herring, S. W., & Mucci, R. J. (1991). In vivo strain in cranial sutures: The zygomatic arch. *Journal of Morphology*, 207(3), 225–239 http://www.ncbi.nlm.nih.gov/entrez/query.fcgi?cmd=Retrieve&db=PubMed&dopt=Citation&list_uids=1856873

Herring, S. W., Muhl, Z. F., & Obrez, A. (1993). Bone growth and periosteal migration control masseter muscle orientation in pigs (Sus scrofa). *The Anatomical Record*, 235(2), 215–222. https://doi.org/10.1002/ar.1092350205

Herring, S. W., & Teng, S. (2000). Strain in the braincase and its sutures during function. *American Journal of Physical Anthropology*, 112(4), 575–593 http://www.ncbi.nlm.nih.gov/entrez/query.fcgi?cmd=Retrieve&db=PubMed&dopt=Citation&list_uids=10918130

Hogg, R. T., & Elokda, A. (2021). Quantification of enamel decussation in gracile and robust capuchins (*Cebus, Sapajus*, Cebidae, Platyrrhini). *American Journal of Primatology*, 83(5), e23246. https://doi.org/10.1002/ajp.23246

Hothorn, T., Bretz, F., & Westfall, P. (2008). Simultaneous inference in general parametric models. *Biometrical Journal*, 50(3), 346–363. https://doi.org/10.1002/bimj.200810425

Hubbard, R. P., Melvin, J. W., & Barodawala, I. T. (1971). Flexure of cranial sutures. *Journal of Biomechanics*, 4(6), 491–496 http://www.ncbi.nlm.nih.gov/entrez/query.fcgi?cmd=Retrieve&db=PubMed&dopt=Citation&list_uids=5162571

Hylander, W. L., Picq, P. G., & Johnson, K. R. (1991). Masticatory-stress hypotheses and the supraorbital region of primates. *American Journal of Physical Anthropology*, 86, 1–36.

Hylander, W. L., Wall, C. E., Vinyard, C. J., Ross, C., Ravosa, M. R., Williams, S. H., & Johnson, K. R. (2005). Temporalis function in anthropoids and strepsirrhines: An EMG study. *American Journal of Biological Anthropology*, 128, 35–56.

Hylander, W. L., & Johnson, K. R. (1985). The relationship between masseter force and masseter electromyogram during mastication in the monkey *Macaca fascicularis*. *Archives of Oral Biology*, 34(9), 713–722.

Izawa, K. (1979). Food and feeding behavior of wild black-capped capuchin (*Cebus apella*). *Primates*, 20, 57–76.

Jaslow, C. R. (1990). Mechanical properties of cranial sutures. *Journal of Biomechanics*, 23(4), 313–321 http://www.ncbi.nlm.nih.gov/entrez/query.fcgi?cmd=Retrieve&db=PubMed&dopt=Citation&list_uids=2335529

Jaslow, C. R., & Biewener, A. A. (1995). Strain patterns in the horncores, cranial bones and sutures of goats (*Capra hircus*) during impact loading. *Journal of Zoology*, 235, 193–210.

Khonsari, R. H., Olivier, J., Vigneaux, P., Sanchez, S., Tafforeau, P., Ahlberg, P. E., Di Rocco, F., Bresch, D., Corre, P., Ohazama, A., Sharpe, P. T., & Calvez, V. (2013). A mathematical model for mechanotransduction at the early steps of suture formation. *Proceedings of the Biological Sciences*, 280, 20122670.

Kinzey, W. G. (1974). Ceboid models for the evolution of hominoid dentition. *Journal of Human Evolution*, 3, 193–203.

Kuznetsova, A., Brockhoff, P. B., & Christensen, R. H. B. (2017). lmerTest package: Tests in linear mixed effects models. *Journal of Statistical Software*, 82(13), 9050–9055. https://doi.org/10.18637/jss.v082.i13

Laird, M. F., Granatosky, M. C., Taylor, A. B., & Ross, C. F. (2020). Muscle architecture dynamics modulate performance of the superficial anterior temporalis muscle during chewing in capuchins. *Scientific Reports*, 10(1), 1–13. https://doi.org/10.1038/s41598-020-63376-y

Laird, M. F., Iriarte-Diaz, I., Byron, C. D., Granatosky, M. C., Taylor, A. B., & Ross, C. F. (In prep). Regional differences in superficial temporalis architecture dynamics in tufted capuchins during chewing.

Laird, M. F., Wright, B. W., Rivera, A. O., Fogaça, M. D., van Casteren, A., Fragaszy, D. M., Izar, P., Visalberghi, E., Scott, R. S., Strait, D. S., Ross, C. F., & Wright, K. A. (2020). Ingestive behaviors in bearded capuchins (*Sapajus libidinosus*). *Scientific Reports*, 10(1), 1–15. https://doi.org/10.1038/s41598-020-77797-2

Lieberman, D. E., Krovitz, G. E., Yates, F. W., Devlin, M., & St. Claire, M. (2004). Effects of food processing on masticatory strain and craniofacial growth in a retrognathic face. *Journal of Human Evolution*, 46(6), 655–677. https://doi.org/10.1016/j.jhevol.2004.03.005

Markey, M. J., Main, R. P., & Marshall, C. R. (2006). In vivo cranial suture function and suture morphology in the extant fish *Polypterus*: Implications for inferring skull function in living and fossil fish. *The Journal of Experimental Biology*, 209(Pt 11), 2085–2102. https://doi.org/10.1242/jeb.02266

Markey, M. J., & Marshall, C. R. (2007a). Terrestrial-style feeding in a very early aquatic tetrapod is supported by evidence from experimental analysis of suture morphology. *Proceedings of the National Academy of Sciences of the United States of America*, 104(17), 7134–7138. https://doi.org/10.1073/pnas.0701706104

Markey, M. J., & Marshall, C. R. (2007b). Linking form and function of the fibrous joints in the skull: A new quantification scheme for cranial sutures using the extant fish *Polypterus endlicherii*. *Journal of Morphology*, 268(1), 89–102. https://doi.org/10.1002/jmor.10504

Masterson, T. J. (1997). Sexual dimorphism and interspecific cranial form in two capuchin species: *Cebus albifrons* and *C. apella*. *American Journal of Physical Anthropology*, 104(4), 487–511.

Moazen, M., Curtis, N., O'Higgins, P., Jones, M. E. H., Evans, S. E., & Fagan, M. J. (2009). Assessment of the role of sutures in a lizard skull: A computer modelling study. *Proceedings of the Royal Society B-Biological Sciences*, 276(1654), 39–46. https://doi.org/10.1098/rspb.2008.0863

Monteiro, L. R., & Lessa, L. G. (2000). Comparative analysis of cranial suture complexity in the genus *Caiman* (Crocodylia, Alligatoridae). *Brazilian Journal of Biology*, 60(4), 689–694 http://www.ncbi.nlm.nih.gov/entrez/query.fcgi?cmd=Retrieve&db=PubMed&dopt=Citation&list_uids=11241970

Moss, M. L. (1997a). The functional matrix hypothesis revisited. 1. The role of mechanotransduction. *American Journal of Orthodontics and Dentofacial Orthopedics*, 112(1), 8–11.

Moss, M. L. (1997b). The functional matrix hypothesis revisited. 2. The role of an osseous connected cellular network. *American Journal of Orthodontics and Dentofacial Orthopedics*, 112(2), 221–226.

Moss, M. L. (1997c). The functional matrix hypothesis revisited. 3. The genomic thesis. *American Journal of Orthodontics and Dentofacial Orthopedics*, 112(3), 338–342.

Moss, M. L. (1997d). The functional matrix hypothesis revisited. 4. The epigenetic antithesis and the resolving synthesis. *American Journal of Orthodontics and Dentofacial Orthopedics*, 112(4), 410–417.

Opperman, L. A. (2000). Cranial sutures as intramembranous bone growth sites. *Developmental Dynamics*, 219(4), 472–485 http://www.ncbi.nlm.nih.gov/entrez/query.fcgi?cmd=Retrieve&db=PubMed&dopt=Citation&list_uids=11084647

Oudhof, H. A., & van Doorenmaalen, W. J. (1983). Skull morphogenesis and growth: Hemodynamic influence. *Acta Anatomica (Basel)*, 117(3), 181–186 http://www.ncbi.nlm.nih.gov/entrez/query.fcgi?cmd=Retrieve&db=PubMed&dopt=Citation&list_uids=6650112

Panagiotopoulou, O., Iriarte-Diaz, J., Mehari Abraha, H., Taylor, A. B., Wilshin, S., Dechow, P. C., & Ross, C. F. (2020). Biomechanics of the mandible of *Macaca mulatta* during the power stroke of mastication: Loading, deformation, and strain regimes and the impact of food type. *Journal of Human Evolution*, 147, 102865. https://doi.org/10.1016/j.jhevol.2020.102865

Persson, M. (1995). The role of sutures in normal and abnormal craniofacial growth. *Acta Odontologica Scandinavica*, 53(3), 152–161 http://www.ncbi.nlm.nih.gov/entrez/query.fcgi?cmd=Retrieve&db=PubMed&dopt=Citation&list_uids=7572090

Popowics, T. E., & Herring, S. W. (2007). Load transmission in the nasofrontal suture of the pig, *Sus scrofa*. *Journal of Biomechanics*, 40(4), 837–844. https://doi.org/10.1016/j.jbiomech.2006.03.011

R Core Team. (2020). *R: A language and environment for statistical computing*. R Foundation for Statistical Computing https://www.R-project.org/

Rafferty, K. L., & Herring, S. W. (1999). Craniofacial sutures: Morphology, growth, and in vivo masticatory strains. *Journal of Morphology*, 242(2), 167–179 http://www.ncbi.nlm.nih.gov/entrez/query.fcgi?cmd=Retrieve&db=PubMed&dopt=Citation&list_uids=10521876

Rafferty, K. L., Herring, S. W., & Marshall, C. D. (2003). Biomechanics of the rostrum and the role of facial sutures. *Journal of Morphology*, 257(1), 33–44 http://www.ncbi.nlm.nih.gov/entrez/query.fcgi?cmd=Retrieve&db=PubMed&dopt=Citation&list_uids=12740894

Rak, Y. (1978). The functional significance of the squamosal suture in *Australopithecus boisei*. *American Journal of Physical Anthropology*, 49, 71–78.

Rak, Y., & Kimbel, W. H. (1991). On the squamosal suture of Knm-Wt-17000. *American Journal of Physical Anthropology*, 85, 1–6.

Ram, Y., & Ross, C. F. (2018). Evaluating the triplet hypothesis during rhythmic mastication in primates. *Journal of Experimental Biology*, 221, 1–10. https://doi.org/10.1242/jeb.165985

Ravosa, M. J., Vinyard, C. J., Gagnon, M., & Islam, S. A. (2000). Evolution of anthropoid jaw loading and kinematic patterns. *The American Journal of Physical Anthropology*, 112, 493–516 http://www.ncbi.nlm.nih.gov/entrez/query.fcgi?cmd=Retrieve&db=PubMed&dopt=Citation&list_uids=10918126

Reed, D. A., & Ross, C. F. (2010). The influence of food material properties on jaw kinematics in the primate, *Cebus*. *Archives of Oral Biology*, 55(12), 946–962. https://doi.org/10.1016/j.archoralbio.2010.08.008

Ross, C. F., Berthaume, M. A., Dechow, P. C., Iriarte-Diaz, J., Porro, L. B., Richmond, B. G., Spencer, M., & Strait, D. (2011). In vivo bone strain and finite-element modeling of the craniofacial haft in catarrhine primates. *Journal of Anatomy*, 218(1), 112–141.

Ross, C. F., & Hylander, W. L. (1996). In vivo and in vitro bone strain in the owl monkey circumorbital region and the function of the postorbital septum. *American Journal of Physical Anthropology*, 101(2), 183–215.

Ross, C. F., & Hylander, W. L. (2000). Electromyography of the anterior temporalis and masseter muscles of owl monkeys (*Aotus trivirgatus*) and the function of the postorbital septum. *American Journal of Physical Anthropology*, 112(4), 455–468.

Ross, C. F., Iriarte-Diaz, J., Reed, D. A., Stewart, T. A., & Taylor, A. B. (2016). In vivo bone strain in the mandibular corpus of *Sapajus* during a range of oral food processing behaviors. *Journal of Human Evolution*, *98*, 36–65. https://doi.org/10.1016/j.jhevol.2016.06.004

Ross, C. F., Reed, D. A., Washington, R. L., Eckhardt, A., Anapol, F., & Shahnoor, N. (2009). Scaling of chew cycle duration in primates. *American Journal of Physical Anthropology*, *138*(1), 30–44.

Roth, D. M., Souter, K., & Graf, D. (2022). Craniofacial sutures: Signaling centres integrating mechanosensation, cell signaling, and cell differentiation. *European Journal of Cell Biology*, *101*, 151258.

Silva, J. d. S., Jr. (2001). *Especiação nos macacos-prego e caiararas, gênero Cebus Erxleben, 1777 (Primates, Cebidae). PhD*. Universidade Federal do Rio de Janeiro.

Silva, J. d. S., Jr. (2002). Sistemática dos macacos –prego e caiararas, gênero *Cebus* Erxleben, 1777 (Primates, Cebidae). Livro de Resumos, X Congresso Brasileiro de Primatologia: Amazônia – A Última Fronteira, 35.

Smith, A. L., Benazzi, S., Ledogar, J. a., Tamvada, K., Pryor Smith, L. C., Weber, G. W., Spencer, M. a., Dechow, P. C., Grosse, I. R., Ross, C. F., Richmond, B. G., Wright, B. W., Wang, Q., Byron, C., Slice, D. E., & Strait, D. S. (2015). Biomechanical implications of intraspecific shape variation in chimpanzee crania: Moving toward an integration of geometric morphometrics and finite element analysis. *The Anatomical Record*, *298*(1), 122–144. https://doi.org/10.1002/ar.23074

Smith, K. K., & Hylander, W. L. (1985). Strain gage measurement of mesokinetic movement in the lizard *Varanus exanthematicus*. *The Journal of Experimental Biology*, *114*, 53–70 http://www.ncbi.nlm.nih.gov/entrez/query.fcgi?cmd=Retrieve&db=PubMed&dopt=Citation&list_uids=4009109

Spencer, M. A. (2003). Tooth-root form and function in platyrrhine seed-eaters. *American Journal of Physical Anthropology*, *122*(4), 325–335 http://www.ncbi.nlm.nih.gov/entrez/query.fcgi?cmd=Retrieve&db=PubMed&dopt=Citation&list_uids=14614754

Sterratt, D., & Vihtakari, M. (2021). RImageJROI: Read 'ImageJ' Region of Interest (ROI) Files_. R package version 0.1.2. https://CRAN.R-project.org/package=RImageJROI

Sun, Z., Liu, Z. J., & Herring, S. W. (2002). Movement of temporomandibular joint tissues during mastication and passive manipulation in miniature pigs. *Archives of Oral Biology*, *47*, 293–305 http://www.ncbi.nlm.nih.gov/entrez/query.fcgi?cmd=Retrieve&db=PubMed&dopt=Citation&list_uids=11922872

Sun, Z. Y., Lee, E., & Herring, S. W. (2004). Cranial sutures and bones: Growth and fusion in relation to masticatory strain. *Anatomical Record Part A-Discoveries in Molecular Cellular and Evolutionary Biology*, *276A*(2), 150–161. https://doi.org/10.1002/ar.a.20002

Taylor, A. B., & Vinyard, C. J. (2009). Jaw-muscle fiber architecture in tufted capuchins favors generating relatively large muscle forces without compromising jaw gape. *Journal of Human Evolution*, *57*(6), 710–720. https://doi.org/10.1016/j.jhevol.2009.06.001

Teaford, M. F. (1985). Molar microwear and diet in the genus *Cebus*. *American Journal of Physical Anthropology*, *66*(4), 363–370.

Teaford, M. F., Ungar, P. S., Taylor, A. B., Ross, C. F., & Vinyard, C. J. (2020). The dental microwear of hard-object feeding in laboratory *Sapajus apella* and its implications for dental microwear formation. *American Journal of Physical Anthropology*, *171*(3), 439–455. https://doi.org/10.1002/ajpa.24000

Theriault, B. R., Reed, D. a., & Niekrasz, M. a. (2008). Reversible medetomidine/ketamine anesthesia in captive capuchin monkeys (*Cebus apella*). *Journal of Medical Primatology*, *37*(Suppl 1), 74–81. https://doi.org/10.1111/j.1600-0684.2007.00267.x

Vinyard, C. J. (2007). Interspecific analysis of covariance structure in the masticatory apparatus of galagos. *American Journal of Primatology*, *69*(1), 46–58.

Vinyard, C. J. (2008). Putting shape to work: Making functional interpretations of masticatory apparatus shapes in primates. In C. J. Vinyard (Ed.), *Primate craniofacial function and biology* (pp. 357–385). Springer Science + Business Media.

Vinyard, C. J., Wall, C. E., Williams, S. H., & Hylander, W. L. (2008). Patterns of variation across primates in jaw-muscle electromyography during mastication. *Integrative and Comparative Biology*, *48*(2), 294–311. https://doi.org/10.1093/icb/icn071

Wall, C. E., Vinyard, C. J., Williams, S. H., Johnson, K. R., & Hylander, W. L. (2008). Specialization of the superficial anterior temporalis in baboons for mastication of hard foods. In C. J. Vinyard (Ed.), *Primate craniofacial function and biology* (pp. 113–124). Springer Science + Business Media.

Wang, Q., Smith, A. L., Strait, D. S., Wright, B. W., Richmond, B. G., Grosse, I. R., Byron, C. D., & Zapata, U. (2010). The global impact of sutures assessed in a finite element model of a macaque cranium. *Anatomical Record*, *293*(9), 1477–1491. https://doi.org/10.1002/ar.21203

Wang, Q., Wood, S. a., Grosse, I. R., Ross, C. F., Zapata, U., Byron, C. D., Wright, B. W., & Strait, D. S. (2012). The role of the sutures in biomechanical dynamic simulation of a macaque cranial finite element model: Implications for the evolution of craniofacial form. *The Anatomical Record: Advances in Integrative Anatomy and Evolutionary Biology*, *295*(2), 278–288. https://doi.org/10.1002/ar.21532

Wickham, H., Averick, M., Bryan, J., Chang, W., McGowan, L., François, R., Grolemund, G., Hayes, A., Henry, L., Hester, J., Kuhn, M., Pedersen, T., Miller, E., Bache, S., Müller, K., Ooms, J., Robinson, D., Seidel, D., Spinu, V., ... Yutani, H. (2019). Welcome to the tidyverse. *Journal of Open Source Software*, *4*(43), 1686. https://doi.org/10.21105/joss.01686

Wright, B. W. (2005). Craniodental biomechanics and dietary toughness in the genus *Cebus*. *Journal of Human Evolution*, *48*(5), 473–492 http://www.ncbi.nlm.nih.gov/entrez/query.fcgi?cmd=Retrieve&db=PubMed&dopt=Citation&list_uids=15857651

Zollikofer, C. P. E., & Weissmann, J. D. (2011). A bidirectional interface growth model for cranial interosseous suture morphogenesis. *Journal of Anatomy*, *219*, 100–114 http://www.pubmedcentral.nih.gov/articlerender.fcgi?artid=3162232&tool=pmcentrez&rendertype=abstract

SUPPORTING INFORMATION

Additional supporting information can be found online in the Supporting Information section at the end of this article.